THE MODULATION COLLIMATOR IN X-RAY ASTRONOMY*

H. BRADT, G. GARMIRE[1], M. ODA[2], G. SPADA[3], and B.V. SREEKANTAN[4]

Laboratory for Nuclear Science,
Massachusetts Institute of Technology,
Cambridge, Mass., U.S.A.

and

P. GORENSTEIN and H. GURSKY

American Science and Engineering,
Cambridge, Mass., U.S.A.

(Received 2 May, 1968)

Abstract. Modulation collimators have been used in recently reported work to determine the angular sizes and celestial positions of the X-ray sources Sco X-1 and Taurus XR-1 (Crab Nebula) with precisions of 15″ to 30″. The measurements were made by means of four-grid collimators, star photography and optical imaging of the collimators. In the present paper we discuss (1) the principles and uses of various forms of the modulation collimators as they pertain to X-ray astronomy, (2) several methods for determining the celestial positions of X-ray sources with these collimators, (3) the techniques for the alignment and calibration of these detection systems, (4) an image-forming collimator, and finally, (5) some of the optical properties of these grid systems. The modulation collimator is quite versatile and is particularly suited for measurements from spacecraft with relatively poor pointing capability. Thus it should be a useful tool in X-ray astronomy for some years to come.

1. Introduction

Measurements of the locations and angular sizes of discrete celestial X-ray sources have been accomplished by several means. In the course of recent work in this field, we have developed and made measurements with new techniques which make use of systems of wire grids to form modulation collimators. The basic device was originally suggested for use in X-ray astronomy by ODA (1965). These collimators are particularly suited for use with the attitude control systems presently available aboard space vehicles and, in particular, aboard sounding rockets. In this paper we discuss these techniques in some detail.

For purposes of comparison, we review briefly two other methods presently in use:

(1) The cellular or slat collimator consists of cells or slits placed in front of proportional counters or Geiger tubes to limit their field of view. The practical lower

* This work was supported in part by the National Aeronautics and Space Administration under contracts NASw-1284 and NASw-1535 and grant NSG-386 and in part by the United States Atomic Energy Commission under contract AT (30-1)2098. In addition, certain portions were carried out at California Institute of Technology under National Aeronautics and Space Administration grant NSG-426 and at the Institute of Space and Aeronautical Sciences, Tokyo.

[1] Present address: Physics Department, California Institute of Technology, Pasadena, Calif., U.S.A.
[2] Present address: Institute of Space and Aeronautical Sciences, University of Tokyo, Tokyo, Japan.
[3] Present address: Laboratorio di Astrofisica, Frascati, Italy.
[4] Present address: Tata Institute of Fundamental Research, Bombay, India.

limit of the field (FWHM) is about $\frac{1}{2}°$. With a precisely constructed collimator and good exposure to a relatively bright source, the centroid of a counting rate peak can be determined to better than 0.1°. In the typical sounding rocket experiment, a decrease of the field width is accompanied by a loss of statistics because, at a given scan angular velocity, the source is viewed for a shorter period. However, as long as the data peak has good statistical significance, the absolute angular accuracy in the centroid position improves. Eventually, uncertainties in the vehicle aspect or imperfections in the collimator geometry, if not the statistics, will limit the precision of a source position. Many of the measurements on the discrete X-ray sources have been accomplished by such means.

(2) A resolution of less than 5″ can be obtained with a focusing telescope whose principle of operation is based upon the reflection of long wavelength ($\geqslant 3$ Å) X-rays from metallic surfaces at grazing incidence angles (GIACCONI and ROSSI, 196[illegible] GIACCONI *et al.*, 1965a). The field of view of these instruments is small ($\sim 1°$). On the other hand, the use of a small X-ray detector in the focal plane can essentially eliminate background counts due to the cosmic ray flux. If X-ray sensitive film or other spatial detectors are placed in the focal plane, high resolution X-ray photographs can be obtained. X-ray photographs of the sun have been obtained with such an arrangement (GIACCONI *et al.*, 1965b; UNDERWOOD and MUNEY, 1967). Also the telescope is ideal for spectroscopic studies of X-ray sources. Since the celestial X-ray sources so far discovered are bright at wavelengths longer than 3 Å, this telescope will prove to be of increasing usefulness in many types of X-ray studies as space platforms with good pointing precision and stability become available.

Oriented space platforms which can be used for X-ray astronomy are of varying degrees of sophistication. The readily available sounding rocket 'attitude control systems' use a gyroscope system which is referenced to inertial space prior to launch. Pointing errors range up to 3° with this system. However, it can be made to scan at rates as low as $10' \text{ sec}^{-1}$ and to 'jitter' about a given orientation with rates of only $1\text{–}3' \text{ sec}^{-1}$. The acquisition of a single optical object (star or sun) can provide more precise pointing ($\sim 2''$) for stellar observations along one axis but with some sacrifice in payload space and weight. In the satellite regime, the sail of the Orbiting Solar Observatory (OSO) can point to a position on the sun with an accuracy of $\sim 1'$. On the other hand, in order to point an instrument at an arbitrary but given celestial position with good precision and with a minimum of drift, jitter, etc., a two-star acquisition system and sophisticated control systems are required. The Apollo Telescope Mount (ATM) will be capable of pointing to any portion of the sun with a precision of about 1″. Comparable or better precision for celestial objects is planned for the Orbiting Astronomical Observatory (OAO), but only for relatively bright stars. The offset pointing precision for OAO (no bright optical object in the field) will be about 1′. These are the only orbiting platforms with three-axis pointing capability with a precision suitable for a grazing incidence telescope, which will become available for some years.

Thus, at the present time, there is a need for detection systems of large area which

require neither good pointing precision nor highly stable platforms, but which determine position and angular size of X-ray sources with high accuracy. One such means is to observe an X-ray source during a lunar occultation. This technique was used successfully to identify the source in Taurus as the Crab Nebula and to obtain its approximate angular size (BOWYER *et al.*, 1964). However, the general usefulness of this method is limited by the infrequency of such fortunate coincidences and by the short duration of each such occultation.

The modulation collimator in its various forms has been developed to meet these needs. In general the collimators have a wide field of view, a relatively large area-time exposure, and the ultimate capability of determining the size of a source down to a few arc seconds. The collimators have multiple angular planes, or 'bands', of transmission so that a source at a large distance is typically viewed many times in the course of a single slow scan. This leads to the accumulation of good statistics which can outweigh the decreased sensitive area due to the wire grids which make up the collimators. When these collimators are used in conjunction with photographic techniques of attitude determination, it is possible in principle to obtain the position on the celestial sphere of a bright X-ray source with a precision of a few arc seconds. For weaker sources, the ambiquity arising from the multiple transmission planes and the obscuration of the counters by the grids tend to make these collimators less effective than slat collimators for measurements of source positions. The modulation collimator, however, is unique in its ability to measure small angular sizes from unstable platforms, even for relatively weak sources.

These techniques were first used in X-ray astronomy to demonstrate that the angular size of the bright source in Scorpio, Sco X-1, is less than 7′ (ODA *et al.*, 1965). Later this upper limit was lowered to 20″ in an experiment which also yielded the celestial position of Sco X-1 with an uncertainty of about 4 square arc minutes (GURSKY *et al.*, 1966a, b). These results led to the optical identification of Sco X-1 as a 13th magnitude, star-like, flickering, ultraviolet object (SANDAGE *et al.*, 1966). X-ray observations of the Crab Nebula during the same flight yielded its angular size and celestial position with a precision of about 20″ (ODA *et al.*, 1967).

The use of a two-grid (bigrid) modulation collimator rotating about its view axis to obtain X-ray source positions in a complex source region has been proposed by MERTZ (1967). The X-ray signals are modulated with frequency components and with a phase characteristic of the source location in the field of view. The resultant time varying signal can be Fourier analyzed to reconstruct the source locations. Recent studies by SCHNOPPER (1968) indicate that under conditions actually encountered in X-ray astronomy, this technique is practical and can offer advantages over other methods. It requires a vehicle with good stability, but good absolute pointing precision is not required. The technique is described in the following paper and thus will not be further discussed herein.

In Section 2 we describe the multigrid collimator, an extension of the principle of the two-grid or bigrid collimator previously described by ODA (1965). It makes possible measurements of angular sizes over a significantly greater range of sizes and

facilitates the determination of source positions. The method of alignment of the multigrid collimator and techniques for the evaluation of its angular response are also presented. In Section 3, we briefly discuss the methods used to construct and evaluate the quality of the wire grids which make up the modulation collimators. In particular, we have developed electroformed grids with wire thicknesses as small as 40 μ. In Section 4, we discuss several techniques for locating the source upon the celestial sphere. In all cases these involve calibration tests to correlate the optical and X-ray response functions. One such test which we have successfully carried out is described. In Section 5, we describe a multigrid collimator which forms an image of the X-ray source on the plane directly behind the collimator. The collimator has potential usefulness in X-ray astronomy when more stable platforms become available. Its effective area remains constant at high X-ray energies and thus it complements the X-ray reflection telescope mentioned earlier. An experimental verification of the principle of this collimator at optical wavelengths is presented.

The alignment and the evaluation of the alignment of the grids in a modulation collimator to precisions of less than one arc minute are by no means trivial tasks. To this end, we have used radiation at optical wavelengths as well as at X-ray wavelengths. Thus we discuss in the Appendix some of the optical properties of these grid systems.

2. Multigrid Collimator

A. BIGRID COLLIMATOR

ODA (1965) described a method wherein a 'modulation collimator' consisting of two wire grids placed in front of an X-ray sensitive Geiger tube or proportional counter could be used to determine the angular size and possibly the angular structure of an X-ray source. In this scheme, illustrated in Figure 1, each grid consists of parallel wires of diameter d and center-to-center spacing $2d$. If incident parallel radiation, such as from a point source at a great distance, falls upon the first grid, then, depending upon the angle of incidence, the portions of the beam which are transmitted by the first grid can fall solely upon the wires, or solely upon the open spaces, or upon both wires and spaces of the second grid. The transmission of the grid system in the first two cases in 0% and 50% respectively and, in the latter case, varies linearly with incident angle.

Thus, the net angular response of the ideal two-grid or bigrid modulation collimator to a parallel X-ray beam is cyclic and triangular in shape with a peak transmission of 50% as illustrated in Figure 2a. The response angle is defined as the full width at one-half maximum, $\theta_r = d/D$, where D is the distance between the grids. The envelope of the triangular peaks (dotted line in Figure 2a) is determined by the collimating effects of the grid enclosure or external metallic slats which, in general, slowly modulate the height of the peaks. The directions for 50% transmission shown in Figure 1a are planes in three-dimensional space. At large distances from the collimator, all such planes which are parallel to one another can be considered as a single plane of maximum transmission (PMT). Each PMT differs from other PMT only because of

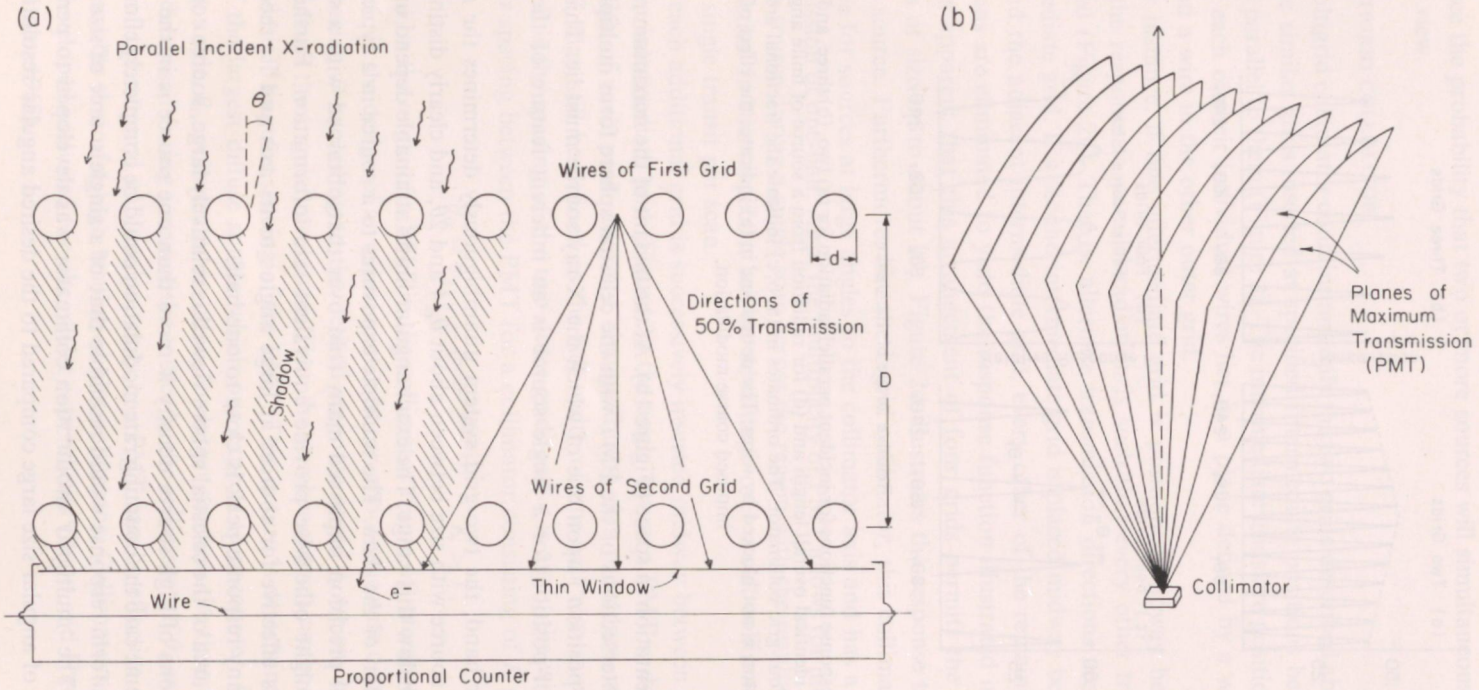

Fig. 1. (a) Geometry of the bigrid modulation collimator, illustrated for incident parallel radiation. To the left, the regions which are blocked to X-radiation by the grid wires are shadowed. At the incident angle shown the net transmission is about 25%. To the right, a few of the incident directions which yield maximum transmission (50%) are indicated. This grid system does not modulate incident radiation if the angular size of the source is greater than about $2d/D$. (b) The planes of maximum transmission (PMT) at large distances from the collimator.

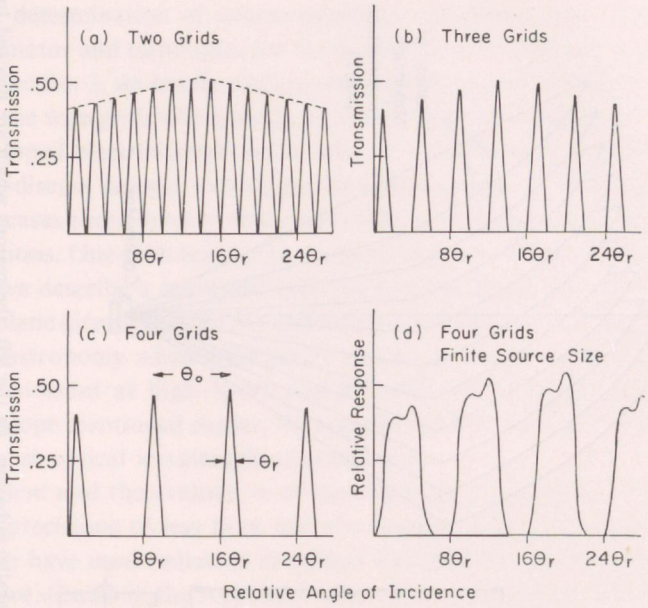

Fig. 2. Angular response functions for incident parallel radiation for (a) two, (b) three, and (c) four-grid collimators of identical overall length and (d) for radiation from a source of finite angular size incident upon the four-grid collimator. The ordinates in (a, b, c) indicate the fractional area which, in the ideal collimator, is not blocked by wires. The dotted line in (a) indicates the effect of a superimposed coarse modulation.

its particular orientation in space (Figure 1b). At the instant of the maximum rate in a data peak, the intersections of the PMT with the celestial sphere form multiple great circles ('lines-of-position') upon one of which the X-ray source must lie. This multiplicity of lines-of-position for a single source is an inherent feature of the bigrid collimator.

On the other hand, the two-grid system unambiguously determines the angular size of an X-ray source with size between about $\theta_r/4$ and $2\theta_r$ and clearly distinguishes sizes above and below this range. The exact angular limits attainable depend upon the statistical precision of the data. The multiple exposures to a source in a typical scan yield a statistical precision improved many fold over that obtained with a slat collimator which might otherwise provide equivalent size information. Furthermore, this collimator is effective for sources at large angles to its axis and its theoretical transmission at any response peak is close to one-half.

Since the net area of the celestial sphere viewed is relatively large, source confusion can arise in regions of high source density if more than one source is in the field of view. In the extreme case the counting rate modulation could be completely eliminated. The resultant uniform response would resemble that of a single source of size greater than about $2\theta_r$. The 'multigrid' modulation collimator was developed to permit the study of sources of angular size large compared to the desired angular resolution and

to reduce the probability that two or more sources will simultaneously lie within the field of view.

B. MULTIGRID COLLIMATOR

The multigrid collimator contains not only the two grids described above but also one or more similar grids inserted at specified intermediate positions between them and aligned parallel to them (Figure 3). The intermediate grids are positioned and rotated so that each of their individual wires lies in a plane defined by a wire in one outer grid and a wire in the other outer grid.

For instance, if one intermediate grid is positioned midway between the outer grids, the response to parallel radiation is such that every other triangular peak is removed (Figure 2b). That is, alternate transmission directions are blocked by the intermediate grid. If a second intermediate grid is placed midway between one outer grid and the adjacent intermediate grid, every other of the remaining transmission directions are eliminated to yield the response function illustrated in Figure 2c.

It is apparent that this arrangement of four grids permits the study of diffuse sources of size up to about $8\theta_r$. Figure 2d illustrates the response to a hypothetical diffuse source. Furthermore, like the bigrid collimator, this collimator also remains effective for sources at large angles to the collimator axis and has a theoretical peak transmission of one-half. Also, the multiplicity of PMT allows for multiple transits of a single source during a single scan across the region with the resultant accumulation of statistics. In this respect it has an advantage over a slat collimator which allows only a single transit per scan.

As each additional grid is successively inserted midway between grid #1 and the adjacent intermediate grid (Figure 3), the angle between PMT is doubled. However the width of each peak does not change during this procedure, and the response angle θ_r may still be defined as the full width of one-half maximum. Thus $\theta_r = d/D$ where D is the spacing of the two outer grids and d is again the wire diameter. The angular spacing between the PMT for a collimator consisting of K grids is:

$$\theta_0 = \phi_{i+1} - \phi_i = 2^{K-1}\theta_r \qquad K > 1,$$

where ϕ_i is the angle of a PMT in the collimator frame of reference.

Thus, in the design of an experiment, one can choose the wire diameter d and outer grid spacing D according to the desired response angle θ_r which, in turn, is usually several times the angular resolution. Then the number of grids can be chosen according to the desired angular spacing of the PMT. This in turn is determined by the angular size of the largest diffuse source which one expects to encounter. Of course, as the spacing angle, θ_0, is increased to allow for larger sources, the time average counting rate is decreased during a scan of the source by the collimator. If θ_0 exceeds the angular width of the external collimation, only one PMT can be effective and the response will resemble that of a high resolution slat collimator. Collimators of this type have been developed and used for ultraviolet experiments (Bedo and Hinteregger, 1965; McGrath, 1968).

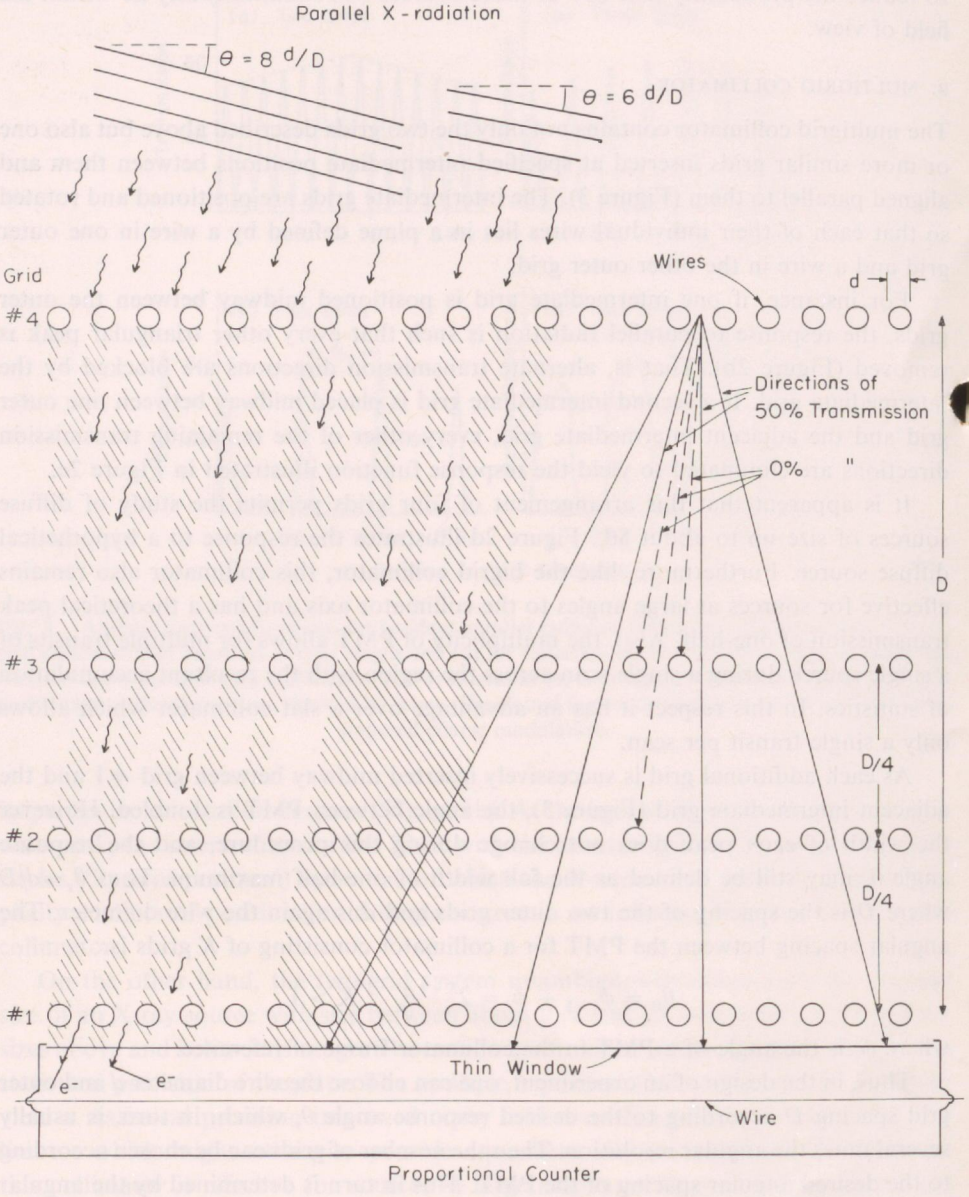

Fig. 3. Principle of operation of the four-grid collimator. To the right, the solid arrows indicate some of the directions of maximum transmission and the dashed arrows indicate some directions of zero transmission. Note that the dashed arrows indicate directions that would be transmitted by grids 1 and 4 in the absence of grids 2 and 3. To the left the shadowing by the wires is shown for two incident directions of parallel radiation, one which yields 50% transmission and the other 0%. The angular response functions in Figures 2a, b, c are for the grid systems containing grids $1+4$, $1+4+3$, and $1+4+3+2$ respectively. The response angle θ_r is defined as the full width at one half the maximum height of the triangular response peak. Thus $\theta_r = d/D$.

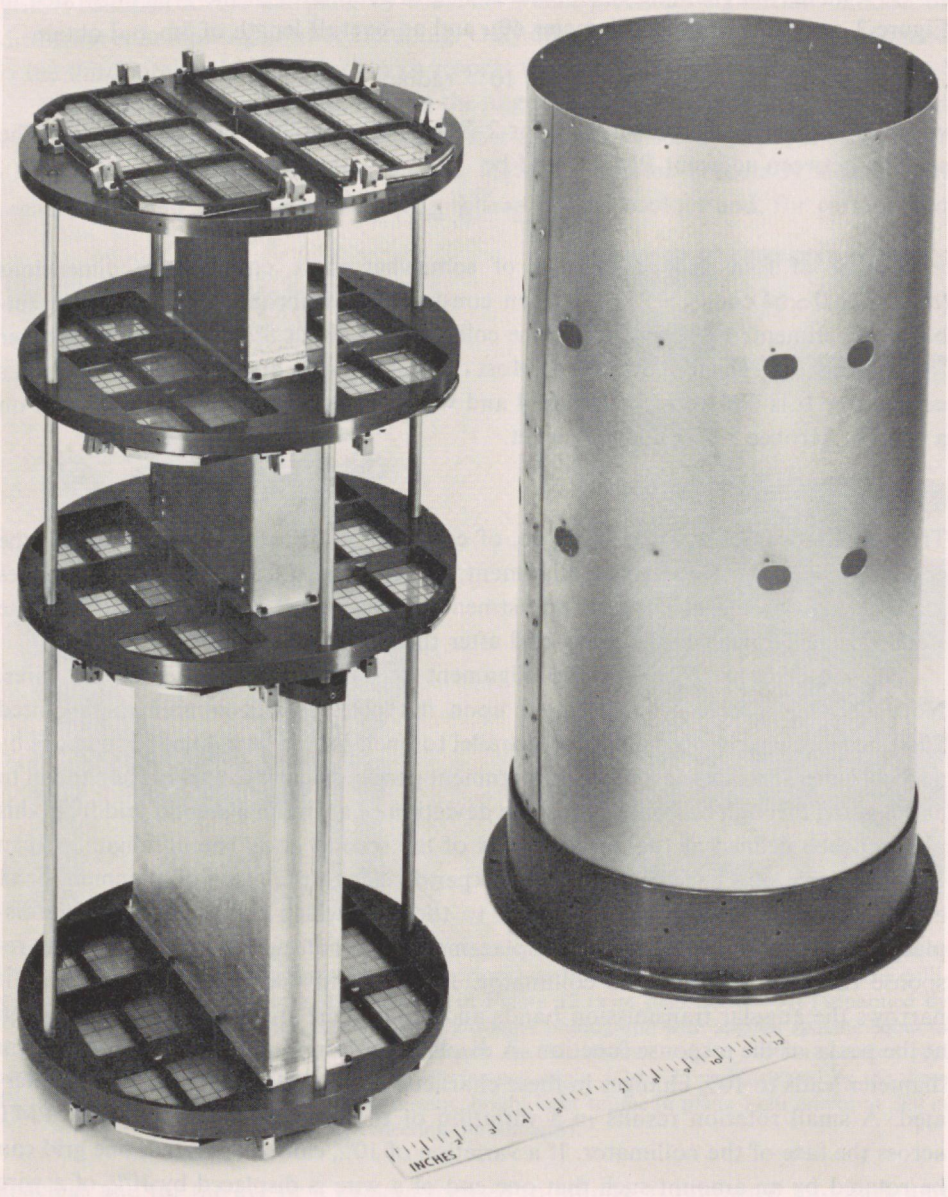

Fig. 4. The double four-grid 'vernier' type collimator described in the text and used for the March 1966 sounding rocket experiment. It is about 30 cm in diameter and 65 cm in length. The entire assembly was housed within the cylinder at the right during alignment and flight. The grids shown in place were electroformed and are similar to that shown in Figure 12, but with 62μ diameter wires. During the actual flight, wire-wound grids with 125μ wires were used. In this flight version, the left collimator was 3 cm longer (66.7 cm) than the right (63.7 cm) to provide the vernier effect. The collimator is shown inverted relative to the schematic in Figure 13, and the fiducial lamps (roughened lucite light pipes) are just under the lower grids.

As a numerical example of an ideal four-grid collimator of the type illustrated in Figure 3, we adopt wires of diameter 40μ and an overall length of 3m and obtain

$$\theta_r = 40/3 \times 10^{-6} \text{ radians} = 2''.7,$$

which is about the diffraction limit for 2–8 Å X-rays passing through 40μ slits. The spacing between adjacent PMT would be

$$\upsilon_0 = 2^{4-1}\theta_r = 21''.6.$$

A pair of four-grid collimators of somewhat more conservative dimensions ($d = 125\mu$, $D \simeq 64$ cm, $\theta_0 \simeq 5'.3$) has been constructed within one frame for a rocket-borne experiment. The length D of one collimator is about 5% longer than the other for reasons to be given in Section 4. Most of the following discussion pertains to this collimator. It is illustrated in Figure 4 and was flown successfully in March 1966 on a NASA Aerobee 150 sounding rocket.

C. GRID ALIGNMENT

The relative positions of the grids are, of course, critical to proper operation of the collimator. To effect the required alignment, one must consider not only the techniques for carrying out the mechanical adjustments but also the means of evaluating the state of the alignment both during and after the adjustment procedure.

The required precision for the alignment is set by the diameter of the wires. Normally the grids will be mounted upon flat plates which contain the required apertures and which are maintained parallel to one another with fixed separations by a rigid frame. If we define a plane of alignment perpendicular to a grid, and parallel to and passing through one of its wires, the deviation of a wire in a second grid from this plane can be defined as the misalignment of the second grid, The misalignment can be in the form of a fixed displacement perpendicular to the plane of alignment or of a rotation about an axis perpendicular to the grid which results in a varying displacement along the wire. A fixed displacement does not modify the shape of the response function of the bigrid collimator. However, in the multigrid collimator, it narrows the angular transmission bands and reduces the area of X-ray transmission at the peaks of the response function. A displacement on the order of 10% of the wire diameter leads to 10% changes in these characteristics, which in general can be tolerated. A small rotation results in a variation of the orientation of the (local) PMT across the face of the collimator. If a variation of 10% can be tolerated, one grid can be rotated by an amount such that one end of a wire is displaced by 10% of a wire diameter from the alignment plane while, for instance, the other end remains in the plane. In terms of a real collimator, e.g. the one flown on the March 1966 rocket flight and described above, a displacement error of 12.5μ could be tolerated. Since the length of the wires comprising the grids was ~ 10 cm, a rotation error of about $\frac{1}{3}'$ was acceptable.

These alignment tolerances can be met with conventional mechanical devices, or, more simply, the necessary adjustments can be made manually. After adjustment, the

grid is clamped to the flat plate by a means which precludes significant motion or distortion either during or after clamping. Only after the first pair of grids are aligned is the third mounted and aligned with respect to the pair, and then the fourth, etc.

During this adjustment, the state of the alignment must be continually monitored by the person performing the adjustment. Certain early observations of the character of optical waves diffracted through the bigrid collimator (Figure 5) suggested a means for doing this. We noted that a diffuse optical background, for certain grid

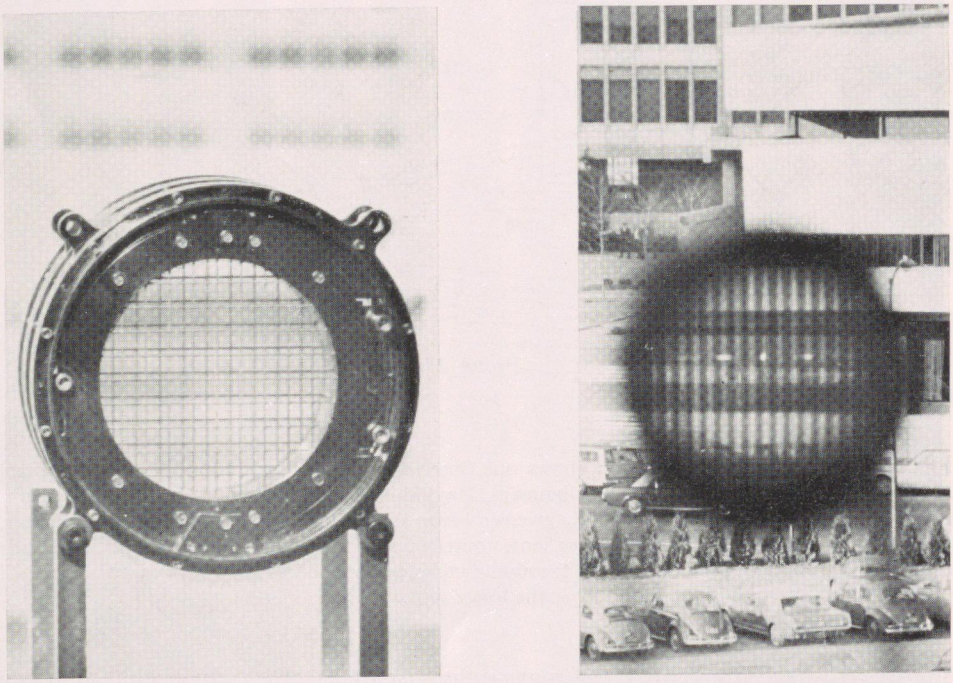

Fig. 5. Photographs with bigrid collimator in foreground with the camera focused on the collimator (left) and at infinity (right). In both cases the aperture was $f/5.6$ and Tri-X film was used. The collimator consisted of two of the grids illustrated in Figure 12 (wire diameter $d = 37\mu$) separated by $D = 3.0$ cm. Note the diffraction bands in the right-hand photograph with angular spacing equal to the Moiré angle $\theta_0 = 2\theta_r = 2d/D = 8'.7$. The bands are this distinct only at certain specified grid separations (see Appendix). The multi-slit interference angle $\lambda/2d \simeq 25'$ is illustrated by the three Fraunhofer diffracted images of a small, distant, bright light source (a plane 5-cm mirror at 300 m reflecting the sunlight).

spacings and for the eye or a camera focused to infinity, is diffracted into dark and light strips of angular separation $\theta_0 = 2d/D$, even though θ_0 is considerably less than the multiple-slit interference angle $\lambda/2d$. Note the diffraction images of the small bright light source in Figure 5.

Figure 6 illustrates the arrangement we have used for the alignment of the multigrid collimator. A diffuse white light source illuminating one side of the collimator is observed through two mirrors with a telescope or theodolite focused on infinity. The mirror is placed at a distance sufficient to allow the entire width of the grids to be in

the field of view. The theodolite serves to resolve and magnify the angles into which the light rays are collimated or, more properly, diffracted by the grid system, and a series of multicolored strips are observed. These patterns can be extremely varied in geometrical or color arrangement depending both upon the wire spacing and the number, spacing, and state of alignment of the grids, and upon the nature of the light

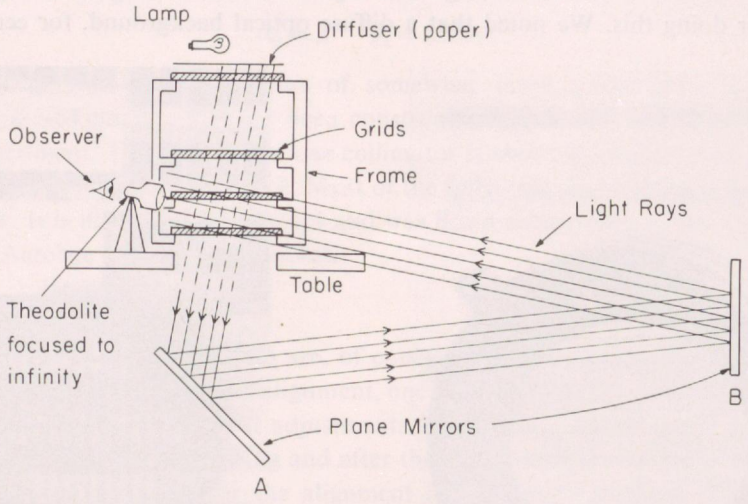

Fig. 6. Physical arrangement which allows one observer simultaneously to adjust grid alignment and to monitor visually the state of alignment. Rays shown are for one of the diffracted beams emanating from the grids. Note that, for a given emission angle, only a small portion of the collimator, of area equal to the theodolite objective lens, contributes to the image. If mirror B is sufficiently distant, the angular field of view of the theodolite includes rays which emanate from all portions of the lower grid.

source. We have found that the many-colored pattern of a diffuse white tungsten light source permits a more sensitive adjustment than the pattern observed with a monochromatic sodium light. Also, we have noted that, occasionally, under certain conditions the patterns are more sharply defined when the aperture of the objective lens of the theodolite is reduced. Further, a small portion of the collimator may be viewed with improved pattern definition if the theodolite is placed only a few centimeters from the collimator. This latter arrangement was used to obtain a photograph taken through the theodolite (Figure 7) of the patterns due to a four-grid collimator.

The relation of these patterns to the state of alignment is not apparent in every respect since the light is diffracted with angles typically many times larger than the collimator angle θ_0. However, in the properly aligned collimator and for light rays at nearly normal incidence to the grids, the observed pattern does repeat itself with a period of θ_0 as expected from the geometrical symmetries. Also, as expected, the pattern is symmetric about the transmission angles which are separated by θ_0. The absence of this symmetry indicates misalignment. It is possible to obtain a symmetric pattern if a grid is displaced a distance d (i.e. 180° in phase) from its proper position;

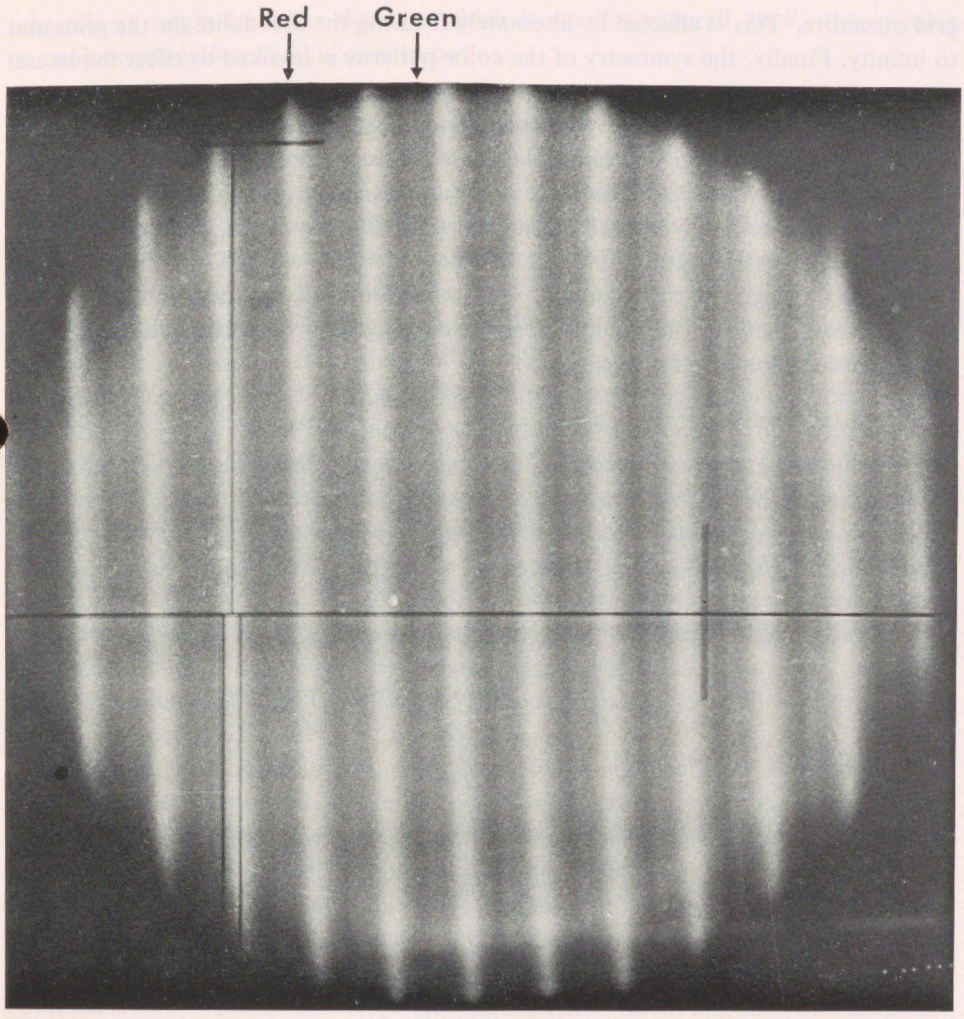

Fig. 7. Photograph of white diffuse light source through an aligned four-grid collimator on Kodak Tri-X film (positive reproduction). A theodolite was used to magnify the image, and in order to obtain good contrast, it viewed the collimator from a distance of only a few centimeters. The angular period of the pattern θ_0 is about 2′.6 and the response angle θ_r about 20″. The light ('exposed') regions appeared visually as bright red and the dark regions as green. The theodolite cross hairs indicate an X-ray transmission direction. Thus for this collimator, the planes of maximum transmission (PMT) are the centers of the light (red) bands.

however an X-ray shadowgraph (see next section) will quickly indicate the misalignment. The nature and colors of the patterns for the proper and improper alignments differ markedly (i.e. red and green versus violet and orange) so only one such shadowgraph is necessary.

Thus, to align a given grid, we first adjust the parallelism of its wires to those of the other grids by requiring that the optical interference pattern be parallel to the

grid structure. This is effected by alternately focusing the theodolite on the grids and to infinity. Finally, the symmetry of the color patterns is invoked to effect the lateral adjustment.

The alignment of the entire system of grids is a difficult procedure and experimentation is required to determine which sequence of mounting and aligning the individual grids yields the clearest color patterns. For certain spacings between grids (D) the pattern may virtually disappear and, as a last resort, one may use a dial gauge to indicate the position of a grid and then rely solely upon X-ray shadowgraphs to indicate the degree of misalignment. It is important to design the collimator so that the grid spacings yield the clearest possible patterns. Empirical trials on an optical bench are sufficient for this purpose.

D. ANGULAR RESPONSE FUNCTION

The testing and calibration of such a collimator usually must be carried out with a point or line X-ray source at a finite distance from the collimator. In this case the collimator may subtend angles from the source which are large compared to the angular spacing of the PMT (Figure 8). If the width of the source is such that it

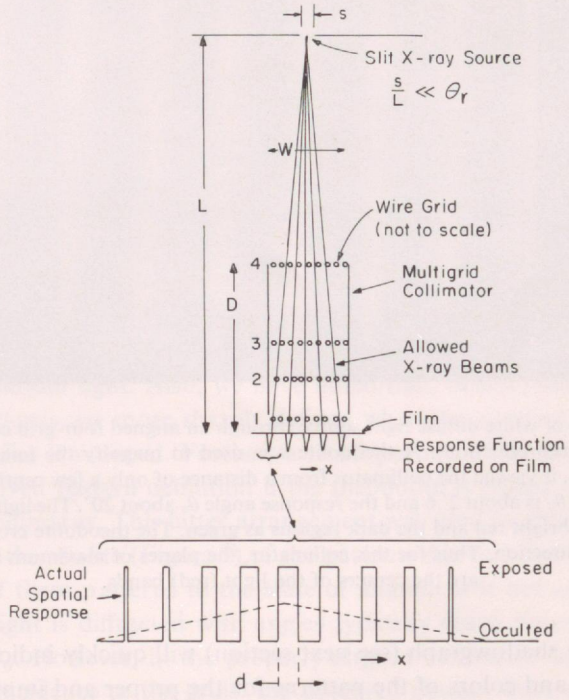

Fig. 8. Physical arrangement for testing response of collimator. Note that the angular response function is transformed into a spatial response function of local average intensity, also triangular in shape. Actually, however, each such triangular peak appears on the film as a series of exposed and occulted regions of widths comparable to the wire diameter d. The drawing is not to scale: the wires are much smaller than shown and, typically, $L \gg D$.

subtends an angle from the detector which is small compared to θ_r, the angular transmission function $P(\phi)$ is seen to be:

$$I(x) \propto F(x) = P\left(\arctan \frac{x}{L}\right),$$

where $I(x)$ is the average local transmitted intensity at position x. Thus we expect the spatial function $F(x)$ for a four-grid collimator to be identical in functional form to the angular response $P(\phi)$ (Figures 2c and 8).

$F(x)$ can be measured by placing X-ray film directly behind the collimator. The value of $F(x)$ is obtained from the resultant shadowgraph by a measure of the local fraction of exposed area. Figure 8 also exhibits, schematically, the expected relative dimensions of the exposed and unexposed regions within a single transmission peak. Note that the pattern reflects directly the occultation by the single wires of the grids. At the center of the response, the X-ray shadows of the wires in each of the four grids are superimposed, and the exposed fractional area, or transmission, is approximately one half. At a slightly displaced position the shadows of the wires in the various grids are no longer superimposed and the increased occultation indicates a reduced effective transmission at the angle associated with this position. Figure 9 is a shadowgraph obtained with a 32 keV X-ray beam illuminating the double four-grid collimator mentioned above ($d = 125\mu$; $D \simeq 64$ cm). The enlarged portion shows the detailed occultation patterns.

The net angular response of a collimator may be obtained from measurements of the widths of the exposed strips in each of many local regions of the shadowgraph. Each such region should yield the expected triangular response. A superposition of these data with the periodicity, $x_0 = L \tan\theta_0$, defined by the overall pattern will yield an angular response function for the collimator as a whole. In such a measurement, care must be taken to superimpose the patterns with the correct periodicity and to take into account the finite size of the X-ray source. The response function so obtained is a superposition of response functions at different angles ϕ_i and each such function is measured for a different region of the collimator. However, the superposition technique should yield an average response function which is closely related to if not identical to the actual angular response for a parallel X-ray beam. This technique becomes easier to apply as the X-ray source is moved to larger distances. The exposed regions on the film become broader and hence encompass more wires. This decreases the required precision of superposition and also permits more measurements of the local transmission within a given transmission peak.

In the limit where the laboratory source is at very large distances ($L > W/\theta_r$, Figure 8) the 50% exposed region will cover the entire photograph if the collimator is oriented so that one of its PMT is coincident with the direction of the X-ray source from the collimator. At the intermediate orientations the photograph will be entirely unexposed. Of course it now becomes possible to replace the photographic film with Geiger tubes or proportional counters to measure directly the angular function

response $P(\phi)$ as a function of detector orientation. The energy of the X-rays must be sufficiently low so that they do not penetrate the wires, and the scattering of the beam in the medium (air or helium) between the source and the collimator must be taken into account. Due to the experimental difficulties, we have not carried out such laboratory measurements on the 64 cm collimator. However, the angular response from a source at large distances can be simulated to a certain extent by a closer source if, as we shall see, the front of the collimator is masked so as to admit X-rays to only a small part of the detector.

The response function of a real detector may differ from the ideal due to either fluctuations or gradual phase shifts of the wire positions on a single grid and also to

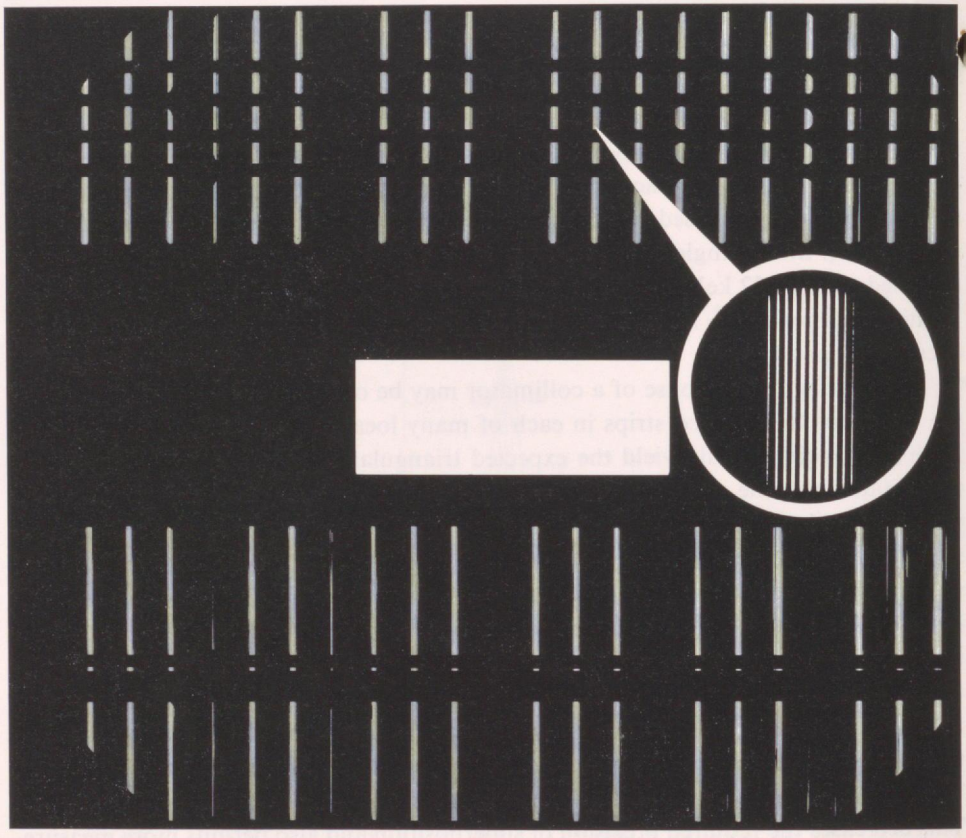

Fig. 9. X-ray shadowgraph (Figure 8) of the aligned double four-grid collimator (Figure 4) immediately after the March 1966 flight (white regions are exposed to X-rays). The grids consist of 125-μ diameter wires and the distance from the source to the collimator was about 7.5 m. The FWHM response angle, θ_r, of the collimator is about 40″ and the angle between PMT, $\theta_0 = 8\theta_r$. The enlargement demonstrates the spatial representation of the triangular angular response function as schematically illustrated in the lower part of Figure 8. The high resolution required to resolve these shadows of the individual wires was obtained in a long exposure without fluorescent screen on standard medical X-ray film. For prompt evaluation of the state of alignment, this resolution is not required, and short exposures with Polaroid X-ray film and with fluorescent screen proved invaluable.

slight misalignments of one grid to another. Clearly, the roughness of the edges of the wires and any bending or bowing of the wires will alter the response function unless these effects are small compared to the wire spacing. The character of this alteration depends upon the nature of the collimator. In general, the response at any one angle is the net transmission of the entire projected area of the collimator. Thus, in a two-grid system, these irregularities will reduce the transmission at the 'transparent' angles and increase it at the opaque angles, thereby reducing the net modulation. In the multi-grid systems the shadows of the wires in the various grids overlap so that minor irregularities tend to narrow the triangular transmission peaks and to reduce the peak transmission. These effects were small for the collimator response shown in Figure 9.

The response of the double four-grid collimator to Sco X-1 during the March 1966 flight is shown in Figure 10. In Figure 11 the superimposed data peaks are compared to the theoretical point-source response. In visible light this object shows no angular extent to a limit of about $\frac{1}{2}''$ (SANDAGE *et al.*, 1966).

3. Grid Fabrication

We have fabricated individual grids for these collimators from copper and tungsten wire. The procedure is to wind the wires around a grooved frame, to secure with epoxy the individual turns of the wire to the frame, and, when the epoxy has set, to strip the wires from one side of the frame. Grids of this type with 125μ diameter wires and of size 10 cm × 25 cm were used in the double collimator flown in March 1966.

We have also had developed* fine mesh electroformed grids which materially increase the resolution of any given collimator. Grids of size up to 30 cm × 25 cm with electroformed nickel and gold 'wires' as narrow as 40μ have been successfully fabricated to meet rocket temperature and vibration specifications. The grids gain mechanical strength from a network of wider electroformed strips running at right angles to the principal patterns and also from an etched 750μ thick copper backing structure.

During flight these grids are held pressed between rigid plates which provide support every 3 to 5 cm. In addition to the fine mesh, these grids exhibit greater uniformity in wire spacing and offer more flexibility in the choice of pattern than is possible with the wire wound grids. On the other hand, they are somewhat more fragile and, because the master must be scribed with a high quality ruling engine, the cost is greater. Also, the extensive supporting structure reduces the transmission from the ideal 50% to about 33% compared to about 40% for a wire wound grid. When a multigrid collimator is used, this latter effect can seriously reduce the effective maximum transmission since the support structures of the several grids are not normally aligned with respect to the X-ray beam. In the case of a collimator with

* Metrigraphics, Inc., Stoneham, Mass.; Buckbee Mears, Inc., St. Paul, Minn. has also successfully fabricated these grids.

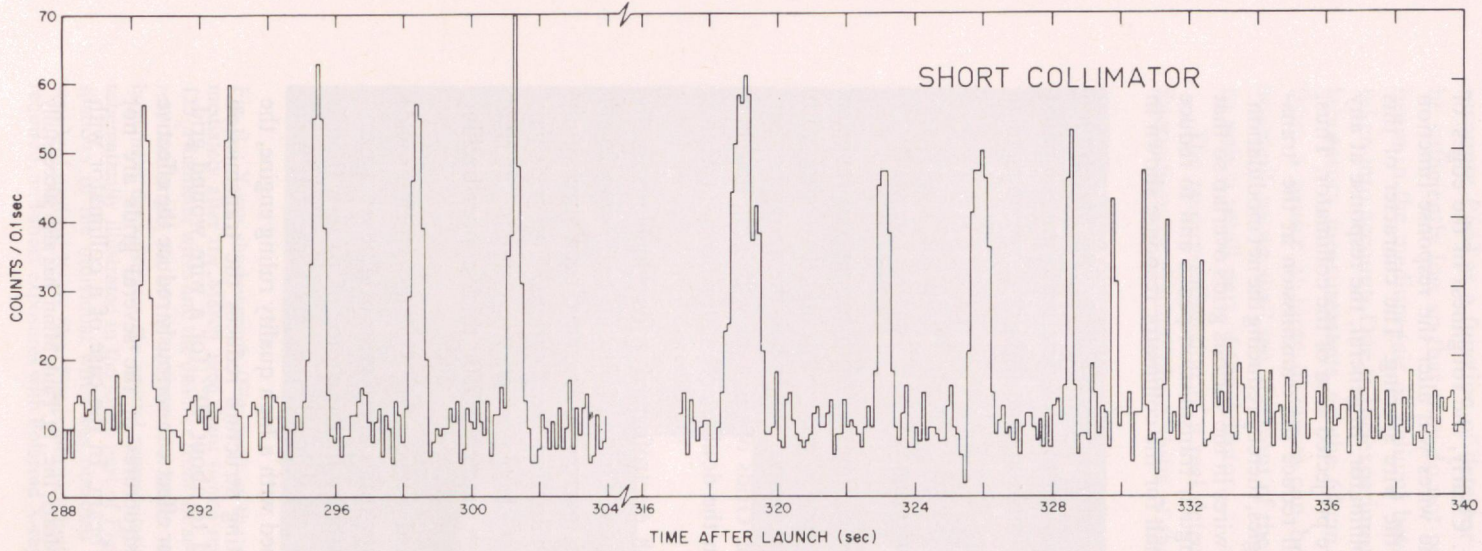
SHORT COLLIMATOR
COUNTS / 0.1 sec
TIME AFTER LAUNCH (sec)
0
10
20
30
40
50
60
70
288
292
296
300
304
316
320
324
328
332
336
340

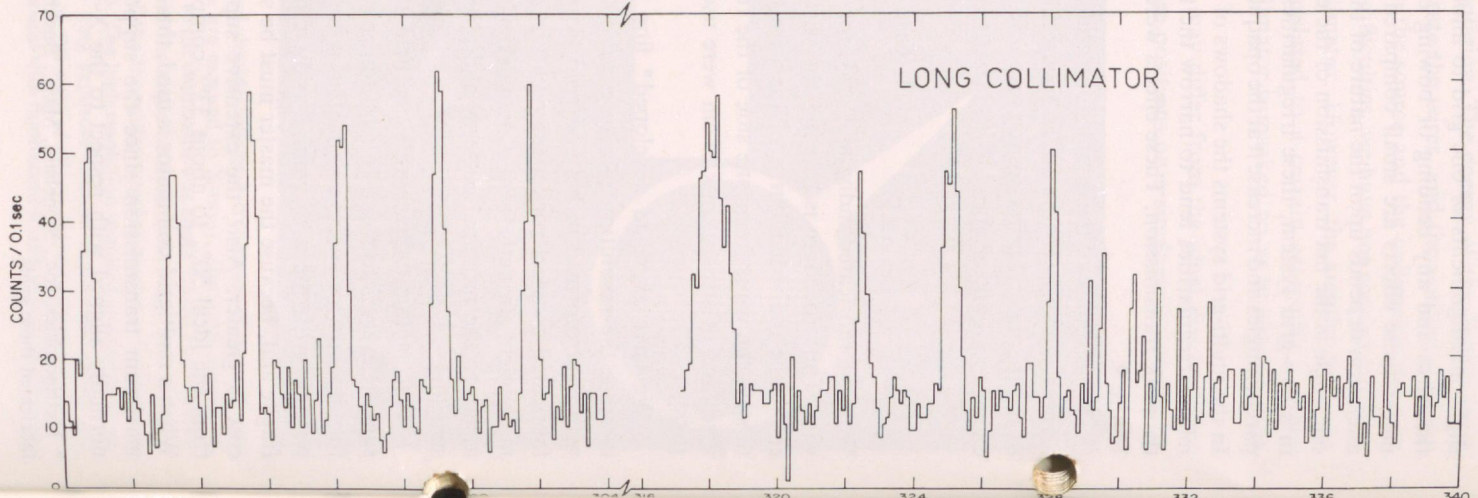
LONG COLLIMATOR
COUNTS / 0.1 sec
0
10
20
30
40
50
60
70

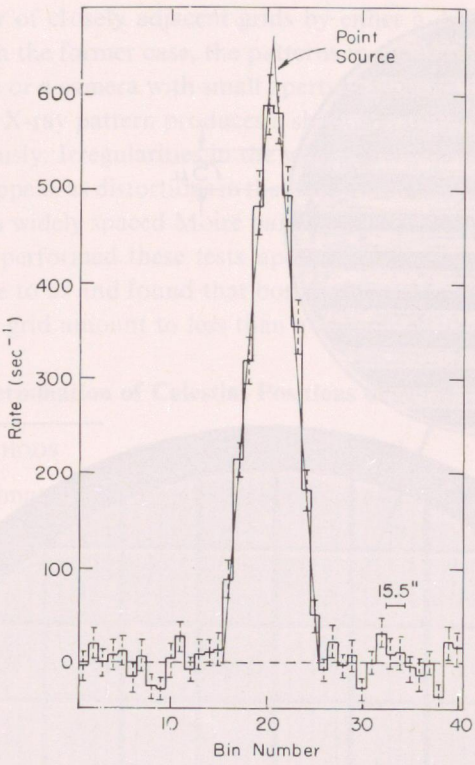

Fig. 11. Superposition of all data obtained during 'hold' portion ($288 < t < 304$ sec) of the Sco X-1 observations (Figure 10).

four of these electroformed grids, the effective peak transmission is about 12% as compared to the ideal 50%. Figure 12 is a photograph of an electro-formed grid.

The intrinsic quality of a grid may be determined in two ways. Local fluctuations in wire spacing may be measured directly with a microscope and micrometer stage. On the other hand, the overall uniformity and phase of the wires may be obtained from examination of the optical or X-ray Moiré pattern which is formed by the

Fig. 10. Histogram of actual counts in the energy range from 1 to 24 keV during the time Sco X-1 was within the field of view of the double collimator shown in Figure 4 during the March 1966 flight. In the frame of reference of the collimator and for $288 < t < 304$ sec, Sco X-1 transited 5 'short' and 6 'long' planes of maximum transmission (PMT) at a uniform rate. It then slowed, stopped and reversed direction, crossing no PMT ($304 < t < 316$), and gradually speeded up crossing two PMT ($316 < t < 324$). At about $t = 324$, a slow roll of the rocket about the view axis was initiated. This motion superimposed upon the linear translation caused Sco X-1 to transit the next PMT rather slowly ($t = 325$–326). Thereafter the fast linear motion increased because the attitude control system lost control as the rocket entered the atmosphere. Note the systematic phase shift of the peaks due to the short collimator relative to those due to the long collimator (e.g. $288 < t < 304$). This relative phase was compared directly with the relative phase of the 'long' and 'short' fiducial bands on the flight film (Figure 14).

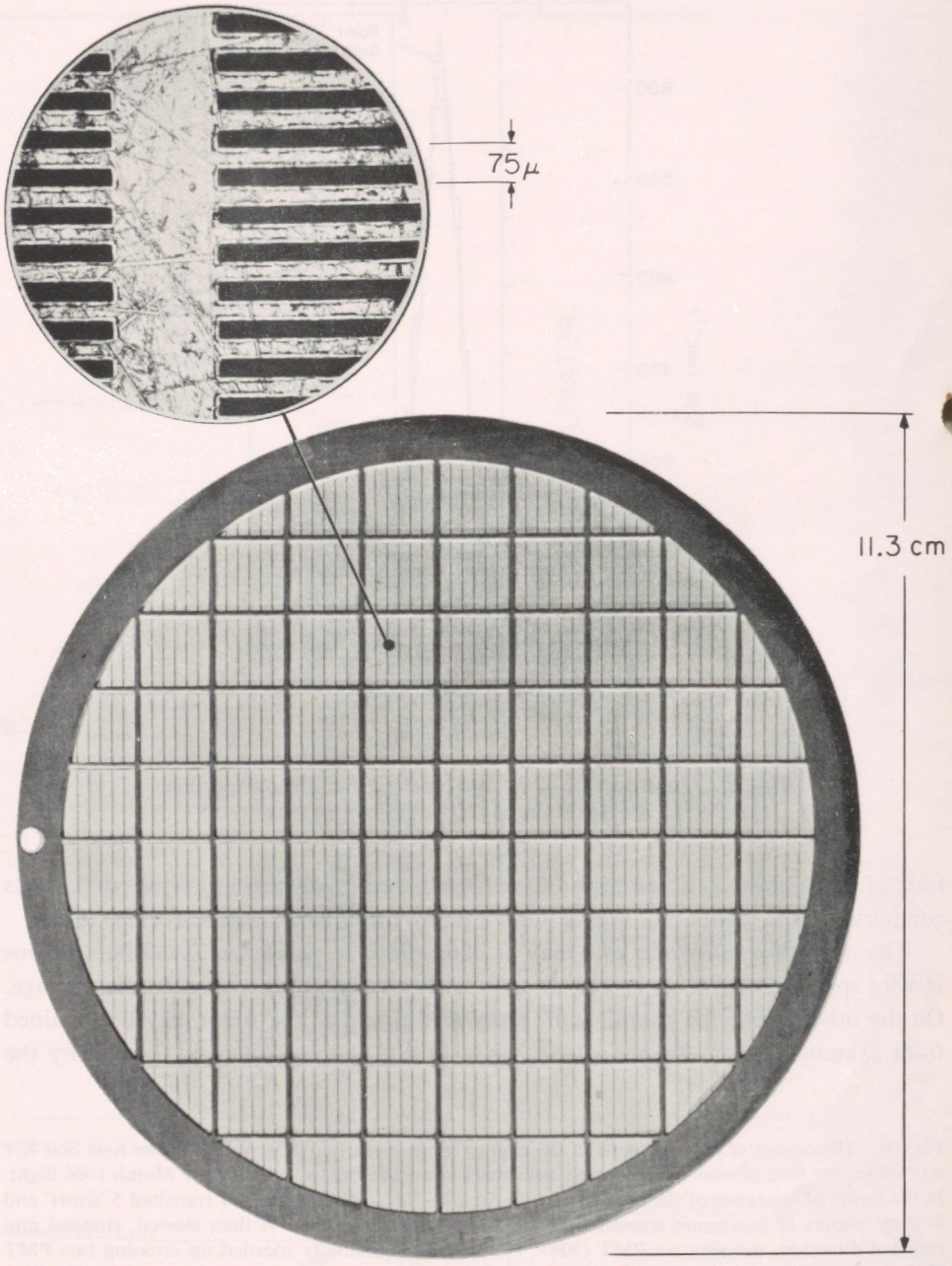

Fig. 12. Photograph of an electro-formed grid; diameter 11.3 cm, wire diameter 37μ. The horizontal Au on Ni wires of thickness $\sim 25\mu$ are electroformed onto a flat Cu plate of thickness 750μ which is then etched from the other side with a selective acid to form a coarse support structure of uniformly spaced ($\sim$ 1 cm) members of cross section $750 \times 750\mu$. The enlargement is a microscopic view of the wires (with polarized light) to illustrate the uniform width and spacing of the 37μ wires. The wider, but thin, electroformed wires which run vertically (see enlargement) provide additional mechanical support. (Grid fabricated by Metrigraphics, Inc.)

illumination of a pair of closely adjacent grids by either a diffuse light source or a point X-ray source. In the former case, the patterns in the transmitted radiation may be resolved by the eye or a camera with small aperture focused at infinity. In the latter case, the transmitted X-ray pattern produces a shadowgraph on X-ray film similar to that described previously. Irregularities in the wire pattern of magnitude comparable to the wire diameter appear as distortions in the Moiré bands of magnitude comparable to their spacing. Thus widely spaced Moiré bands provide the most sensitive measure of irregularities. We performed these tests upon both the wire wound and electroformed grids available to us and found that both fluctuations and systematic shifts of phase over the entire grid amount to less than about 5% of the wire diameter.

4. Determination of Celestial Positions of X-ray Sources

A. EXPERIMENTAL METHODS

The modulation collimator may be used not only to determine the angular size of an X-ray source whose position is known only approximately but also to determine the celestial position of the source. For this latter purpose it is necessary to incorporate certain additional features into the experiment, and it is these which we shall consider in this section.

During the flight of a sounding rocket the modulation collimator can be pointed

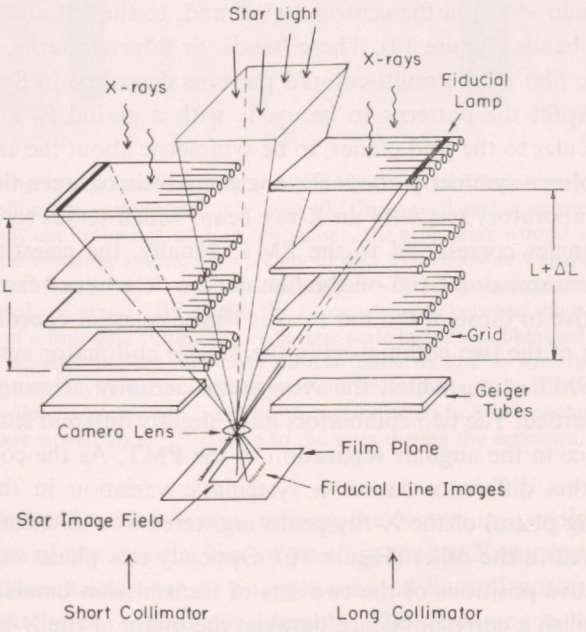

Fig. 13. Schematic of the double or 'vernier' modulation collimator. The vernier technique requires that the angular separation between transmission planes be slightly larger in one collimator than the other. The slightly different lengths of the two collimators provide this effect. The flight collimator constructed according to this principle is shown in Figure 4.

in the direction of the X-ray source to an accuracy of a few degrees and with a jitter which causes the several PMT to transit the source slowly (1–3′ $\sec^{-1}$). At each such transit, the X-ray detector will show a maximum in the counting rate. The precise instant of the maximum is obtained by means of a suitable timing device in the recording system. To obtain the source position, one first determines the celestial coordinates of the several PMT at this instant and secondly identifies the particular PMT which is transmitting X-rays at this instant. The intersection of this PMT with the celestial sphere is the 'line-of-position' for the source. We shall discuss several ways in which these measurements can be carried out.

In the March 1966 flight, a 'double modulation collimator' system was successfully used and the location of the bright X-ray source, Sco X-1, was determined with a precision of about 4 square arc min. The principle underlying this system may be understood by a reference to Figure 13. Two modulation collimators of almost identical design were mounted next to each other with the wires of one aligned to be parallel with the wires of the other. During the flight a 16 mm camera with 50 mm $f/1.4$ lens, mounted below the collimators and focused to infinity, recorded on a common frame of Kodak Tri-X film: (1) the stars that were visible through the rectangular opening between the two collimators and (2) the light passing through the collimators from long, thin diffuse light sources located on the far side of the two collimators. Successive one-second exposures were taken, and the rocket motion was typically 1–3′ $\sec^{-1}$. The record on the photographic film thus consists of trailed star images (magnitude <5.5) in the central region and, to the left and right, two sets of dark and white bands (Figure 14). These bands, or fiducial marks, are the image on black and white film of the multi-colored patterns described in Section 2. Again in this case, we expect the patterns to be cyclic with a period θ_0 and, for directions nearly perpendicular to the grid planes, to be symmetric about the angles of the PMT. This in turn implies a symmetry about the angles midway between the PMT. Later we will describe a laboratory test with an X-ray beam which serves to identify which of the symmetry angles correspond to the PMT. Finally, the celestial coordinates of any particular transmission band on the film can be determined from its coordinates on the film relative to those of the star images whose celestial coordinates are known.

The purpose of the two collimators in the double collimator system is to identify the particular PMT along which the X-rays are actually arriving when an X-ray maximum is recorded. The two collimators have slightly different lengths so that there is a 5% difference in the angular separation of the PMT. As the collimator scans an X-ray source, this difference causes a systematic variation in the angular phase (actually a timing phase) of the X-ray peaks registered in one set of counters relative to those registered in the other (Figure 10). Optically this phase variation manifests itself in the relative positions of the two sets of transmission bands on the film. It is possible to establish a correspondence between the phase of the X-ray peaks and the phase of the transmission bands on the film. That is, the phase of a particular X-ray peak identifies the corresponding transmission band on the film because it exhibits the same phase. The celestial coordinates of the center of this band are the celestial

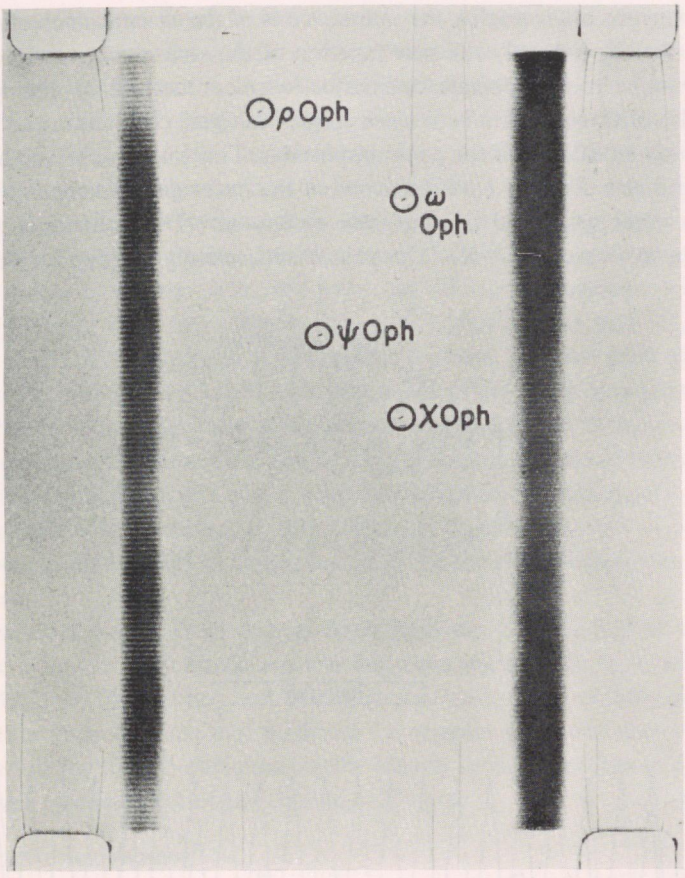

Fig. 14. Flight photograph of star field (star tracks circled) and of fiducial lamps through a double four-grid 'vernier' collimator as illustrated in Figure 13. The overall grid separation was 64 cm in the right collimator and 67 cm in the left, and, in both cases, the grids were wound with 125 μ diameter wire. Thus the angular response angles, θ_r, were about 40″. The exposure was made for one second on Kodak Tri-X film with an $f/1.4$, 50 mm lens. Hence the ~ 78 μ separation between fiducial marks corresponds to an angle of about 320″ or $8\theta_r$ the expected angle between the planes of maximum transmission (PMT) of a four-grid collimator. A precise scale factor was obtained from the star field. Note the difference between the left and right fiducial patterns due to the slightly different grid separations. Also there are asymmetries on the upper and lower parts of the patterns. The upper edge of the film represents directions about 6° from the normal to the grids. The rocket and thus the camera axis moved about 1′ relative to the stars during the exposure.

coordinates of the PMT which is transmitting the X-rays in question. That is, they are the coordinates of the celestial line-of-position for the X-ray source.

By this procedure the number of possible celestial lines-of-position on which the X-ray source might lie is reduced considerably. The remaining multiplicity of lines derives from the reoccurrence of the same phase which, for the collimators under discussion, occurs after about 20 lines or at angular intervals of about 2°. If further scans with good statistical accuracy are made with the collimator rotated about its

view axis to various other angles, the intersections of the several lines-of-position can in principle identify uniquely the true position of the source.

An alternative to this double collimator 'vernier' method of distinguishing the various angles of transmission is to use a single multigrid collimator and to introduce a second gross modulation of the peak amplitudes. This can be achieved by placing an additional grid at a distance D/m from one of the outer grids where D is the distance between the outer grids and m is usually an integer. This scheme is illustrated in Figure 15. In this case $2^{-K+2}m-1$ peaks of successively varying amplitude will be

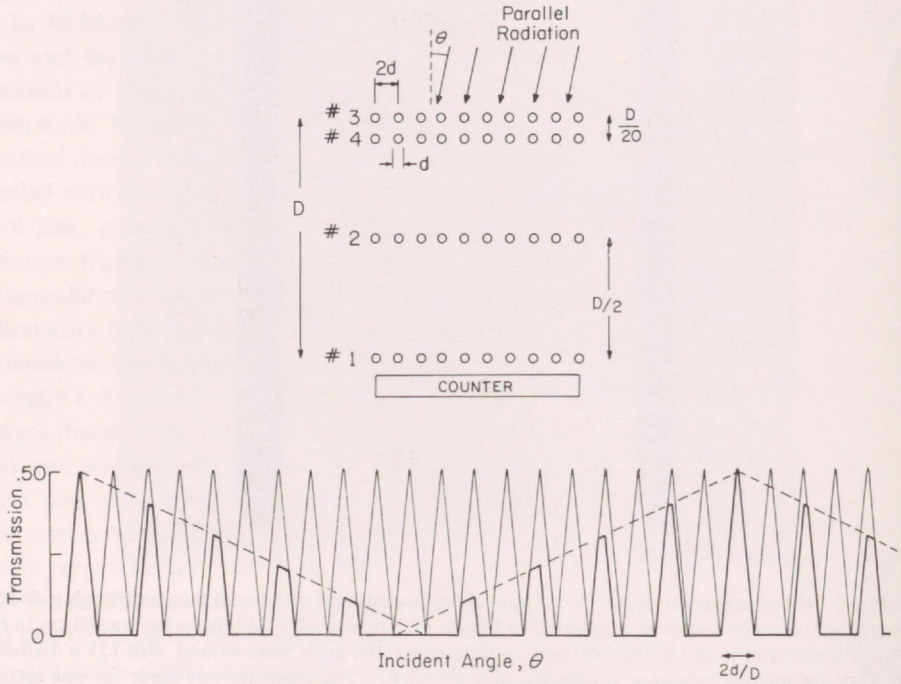

Fig. 15. Transmission of three-grid collimator with additional grid (# 4) at $D/20$ below the top grid to modulate peaks (heavy lines). The narrow triangles (light lines) indicate the response of this grid system if grids # 2 and # 4 are removed.

recorded for each complete cycle of modulation where K is the number of grids in the basic collimator. Also the spacing between the peaks will change continuously as will the shape of the peaks. These features can also be used to distinguish one peak from another. Optically the same features are seen in photographs of a diffuse fiducial lamp taken through the collimator. The advantage of this method is that only one collimator suffices to define the transmission plane corresponding to a given X-ray data peak. On the other hand, the scan might yield only a few data peaks and these could be near a minimum in the superposed modulation pattern. Also, the additional grid reduces the time average transmission of the collimator with a resultant loss of statistics.

It is possible in some cases to photograph the stars through the grids. At any instant, only those stars that happen to lie in certain celestial regions produce a photographic image and, as the collimator-camera system slowly scans the sky, the image of each star is trailed and modulated. The times at which particular stars appear and disappear yield the celestial coordinates of the several PMT at the time of the data peak. The success of this method depends on the technical feasibility of photographing the stars through several grids and the availability of sufficiently bright stars in the vicinity of the source. Diffraction in the fine grids reduces considerably the effective intensity of star light. We have carried out experiments with artificial stars which indicate that for a four-grid system ($D=65$ cm) with 62μ wires the reduction is nearly 10^{-4}, a clearly unacceptable amount. Coarser grids yield a much greater intensity and can be used with either a camera or a lens-photomultiplier recording system. One must take into account the diffraction images of the stars. Typically one obtains the same three bright central images (Figure 5) that are obtained from Fraunhofer diffraction of a plane wave by a single transmission grating with wire spacing twice the wire diameter. If this approach is followed, one of the methods discussed above must be used to determine which of the PMT is operative at the time of a data peak.

Finally we note that if, prior to a given experiment, the celestial position of any X-ray source is known with an uncertainty less than the angular separation between adjacent PMT, then there is no need to reduce the multiplicity of lines of position in order to obtain improved celestial positions or angular structure. For instance, the measurements of the Crab Nebula during the March 1966 flight (Oda *et al.*, 1967) did not require the vernier effect of the double collimator.

B. LABORATORY CALIBRATION

The correlation of the X-ray and optical characteristics of these collimators makes necessary a fundamental calibration experiment. As explained earlier, diffraction effects cause the photographed image of the fiducial lamps to be rather complex. It is therefore necessary to determine which part of the pattern corresponds to the planes of maximum transmission (PMT). For this purpose the following experiment was carried out to calibrate the double four-grid collimator described above.

X-rays from an X-ray generator were collimated by two vertical slits (A and B) separated by about 8 m (Figure 16) and made to pass through the collimator. The collimator was rotated so that its wires were parallel to the slits. The X-rays were detected by proportional counters mounted behind the collimators. The collimator was mounted on a turn table which was rotated until the counters behind one collimator showed a maximum in counting rate. This occurred when one of the PMT was parallel to the plane of the X-ray beam as defined by the two slits, A and B. A point-like optical source C, a small brightly illuminated round hole, was placed just above the X-ray slit A close to the generator so that the optical source C and the slit B defined the same plane for optical radiation as was defined for the X-radiation by the slits A and B. The alignment of the slits and source was carried out with a

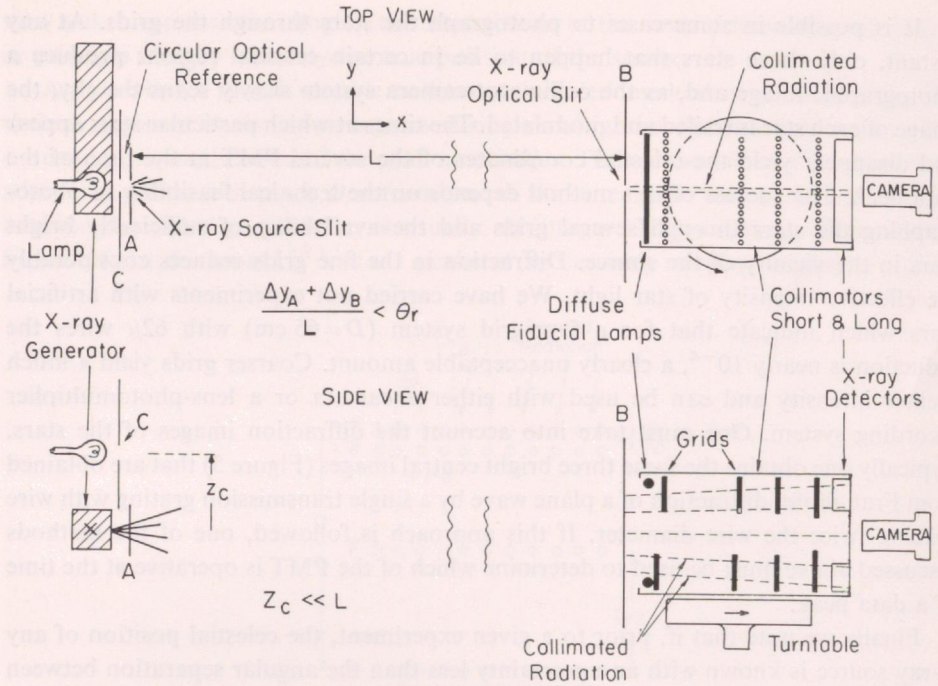

Fig. 16. Fundamental experiment to correlate X-ray transmission directions and the photographic images of the fiducial lamps. The camera of 500 mm focal length is focused to infinity and views both the optical reference source *C* and the fiducial lamps. The X-ray slits *A* and *B* and the source *C* all lie in the same plane, and the grid wires are parallel to the slits. The optical beam is collimated by *C* and *B* and thus not only lies in the same plane as the X-ray beam but appears in focus in the *y* direction because slit *B* effectively reduces the lens aperture in that direction. In our experiment, the collimator resolution, θ_r, was about 40″ and the distance, *L*, about 8 m. Other dimensions are given in the text.

transit located about 20 feet behind the collimator. A 500 mm focal length camera mounted behind the collimator was then used to photograph the collimator fiducial lamps through the grids and simultaneously the bright illuminated optical 'star' *C* through the slit *B* just in front of the collimator.

In such a calibration experiment, the collimation of the optical 'star' rays by slit *B* is necessary since the 'star' is at a finite distance from the camera. The camera has both a wide aperture and its focus at infinity in order to properly photograph the fiducial lamps according to flight conditions. In essence this slit *B* stops down the lens in one dimension to bring the 'star' rays into focus while maintaining the wide aperture for the fiducial lamps. At the same time slit *B*, together with the location of *C*, insures that the optical rays are collimated into the same plane in space as are the X-rays. The photographic image of *C* thus marks the position of the X-ray source relative to the fiducial marks. If the collimator is oriented to allow passage of X-rays with maximum intensity, this image thus marks the portion of the fiducial pattern which corresponds to a PMT. Since the diffracted fiducial rays are multicolored, it is important to use the same type black and white film as will be used in flight.

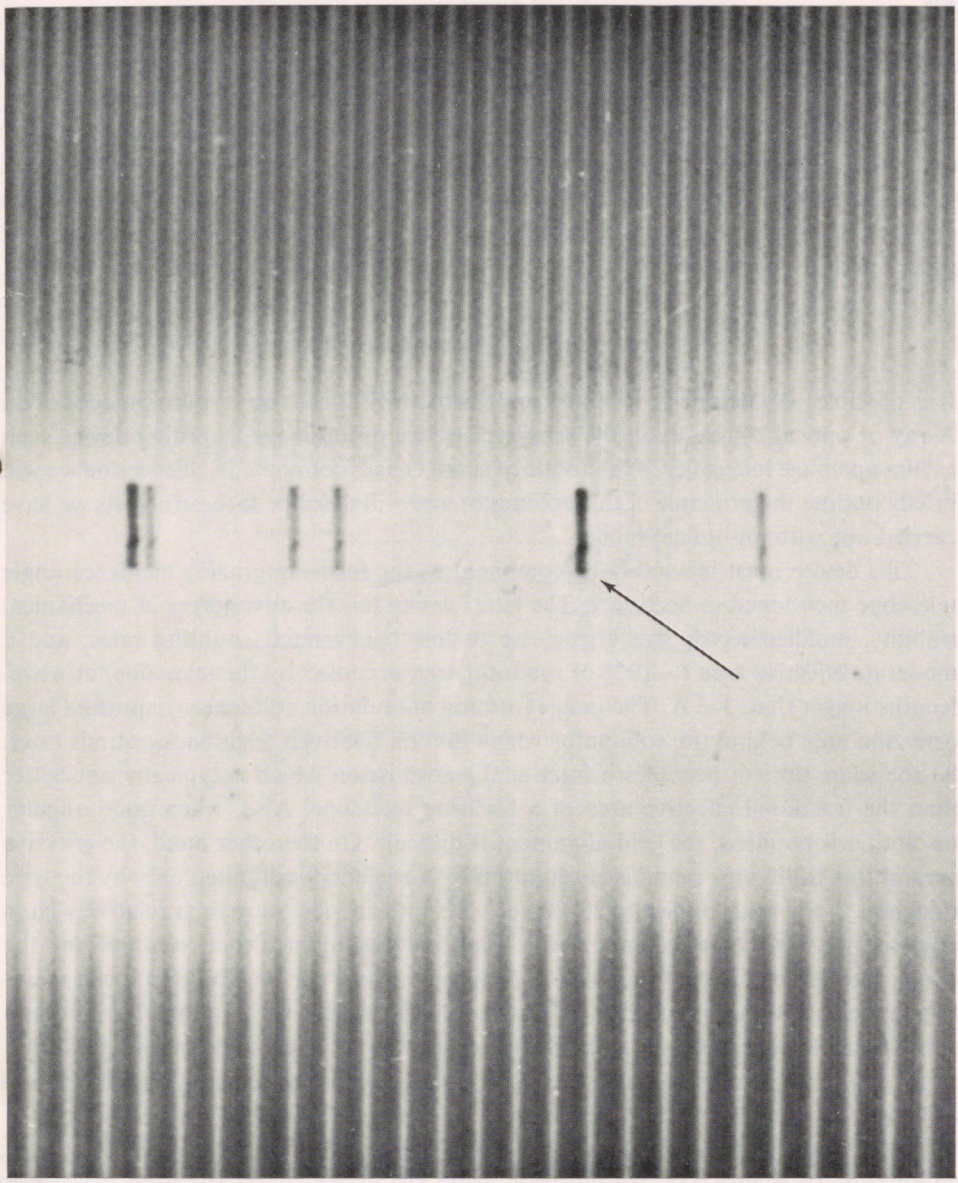

Fig. 17. Photographic result of the fundamental calibration experiment on Tri-X film (negative reproduction) just prior to the March 1966 flight. The details of the experiment are illustrated in Figure 16. The collimators are those used for the flight, and the periodicity of the fiducial marks shown is about 5′. Note the doublet structure of the upper fiducial pattern photographed through the 64 cm (short) collimator in contrast to the pattern below taken through the 67 cm (long) collimator. The photograph was taken with the collimator rotated to an angle such that the grids were approximately normal to the X-ray beam and, furthermore, such that there was a counting rate maximum in the X-ray detectors behind the short collimator. The X-ray source, represented by the optical marker (arrow), lines up with one of the narrow, light (i.e. unexposed) lines in the upper (short) pattern within about 15″, i.e. within 5% of the pattern periodicity. Thus we can conclude from this experiment alone that the narrow, unexposed lines on the film mark the planes of maximum transmission (PMT) of the short collimator within about 15″, for incident X-ray directions approximately normal to the grids.

In the experiment we carried out, the approximate dimensions of slits A and B and source C were 125μ, 0.15 cm, and 650μ respectively and the film used was Kodak Tri-X. Figure 17 is a portion of a photograph obtained when the upper (short) collimator was transmitting X-rays at maximum intensity. The source image C is indicated by an arrow. Note that, as expected, the source appears to line up with a symmetry position in the upper fiducial pattern. Careful measurements indicate the precision of the alignment is better than 5% of the line spacing in the pattern, or $\sim 15''$.

5. Image Forming Modulation Collimator

It is possible to assemble a series of grids which will form one or more images of an X-ray or optical source upon the sensitive surface of an image recording device such as film an image intensifier, or a mosaic of small Geiger counters. In this section we will briefly outline the principle of this collimator and will describe successful tests we have carried out with an optical model.

This device must inevitably be compared to the focusing grazing incidence angle telescope mentioned in Section 1. The latter device has the advantages of mechanical stability, small detector size giving rise to low background counting rates, and a moderate effective area ($\sim 10\%$ of the total area occupied by the telescope) at wavelengths longer than 3–5 Å. The image forming modulation collimator requires a large detection area behind the collimator which implies relatively high backgrounds rates. At the same time, it provides a fractional transmission which is typically not better than the fractional effective area of a focusing telescope. Also, when good angular resolution is required, the grid alignment is difficult. On the other hand, the effective area of this collimator remains constant up to X-ray energies limited only by the wire thickness in the grids, typically 20–30 keV. Also it can view sources at relatively large angles (5–10°) from the collimator axis. Both the grazing incidence telescope and the image forming collimator must be mounted on a rocket or satellite which can maintain its axes stationary with respect to the celestial sphere with an angular precision comparable to that desired for the imaging. However, the absolute pointing requirements are much less severe for the image-forming collimator because of its large field of view.

The image-forming collimator is closely related to the multigrid modulator collimator. In Figure 18a, we illustrate again the experimental situation wherein a point X-ray source illuminates a multigrid collimator placed at a finite distance from the source. The photons from the source can pass through the collimator only along discrete paths to form strip patterns or images upon the recording film. It is clear from the geometry of the collimator (Figure 3) that if n wires lie between adjacent paths of maximum transmission in grid #1, then the number of wires between the same paths in grids 2, 3, and 4 are $n-1$, $n-2$, and $n-4$, respectively. Now we can also construct a collimator (Figure 18b) of four grids of differing wire separations and diameters such that the number of wires between adjacent paths from grid to grid is again n, $n-1$, $n-2$, and $n-4$, and also such that the transmission paths are parallel

to one another. In this case, a plane wave of radiation incident normal to the grids should produce a one dimensional 'strip' multiple image pattern identical to that obtained from the experiment illustrated in Figure 18a. This pattern is shown in Figures 8 and 9. If the plane wave is incident at a slightly inclined angle, it turns out that, not only are there transmission paths through the collimator at this angle, but

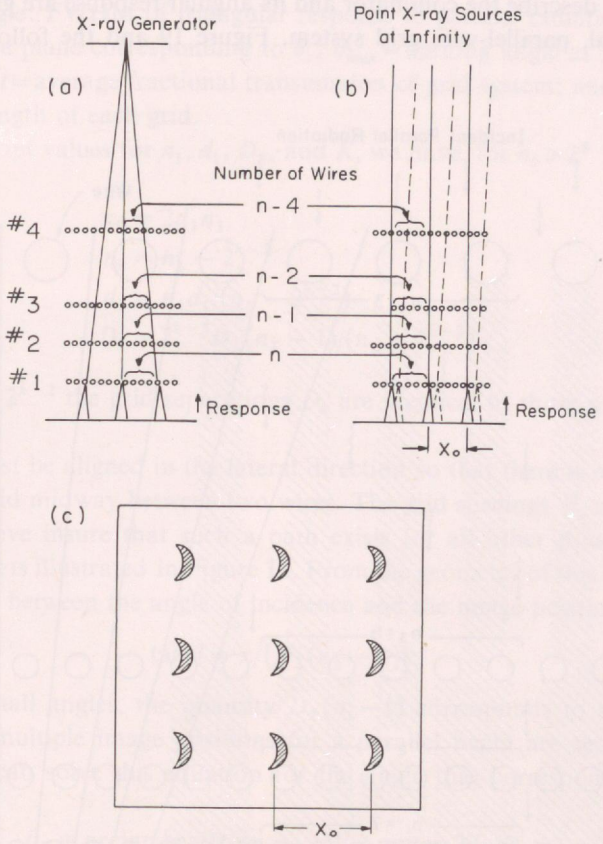

Fig. 18. Comparison of (a) the multigrid collimator and (b) the image forming collimator. (a) As in Figures 8 and 9, the angular response of the multigrid collimator is converted to a spatial response when a point source is placed at a finite distance. In this case, the numbers of wires between adjacent transmission directions in the various grids are $n, n-1, n-2\, n-4$, etc.; (b) If the densities of the wires in the several grids are properly modified and the grids properly aligned, an incident parallel beam can produce the same spatial pattern. If further turns out that parallel beams at other angles create images at displaced positions (dotted lines); (c) Multiple-image pattern expected from a hypothetical exposure to the moon with a two-dimensional image forming collimator.

they are located such that the image is slightly displaced from the image position for normal incidence (dotted patterns in Figure 18b). Thus, an object of finite angular size can be transformed into a series of one dimensional spatial images with regular spacing x_0. If, in addition, each grid is constructed of crossing perpendicular sets of wires with the same uniform density of wires in each direction, a two-dimensional series of images is formed as illustrated in Figure 18c.

We find that, if the number of wires between images is not large compared to 2^{K-2} where K is the number of grids, the spacing of the grids must be modified from that of the multigrid collimator so the wires in the various grids will be properly aligned at all angles. This correction turns out to be important for the optical model we constructed and is taken into account in the following description. The quantitative relations which describe the collimator and its angular response are given here for the one-dimensional, parallel-wire grid system. Figure 19 and the following define the symbols used.

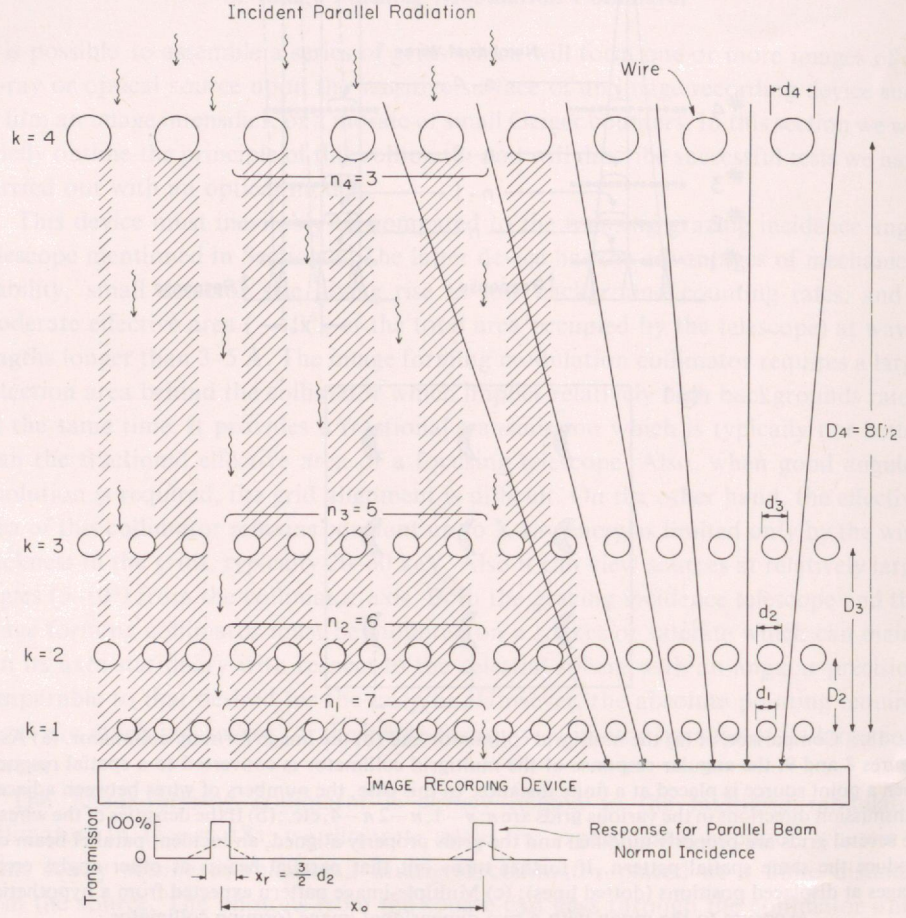

Fig. 19. Four-grid image-forming collimator with 7 wires between multiple transmission directions in the first grid, and 6, 5, and 3 wires in grids 2, 3, 4 respectively. Parallel radiation, incident normal to the grids, produces the shadowing shown at the left and the spatial response shown at the lower left. This response is rectangular in shape because of the small values of n_i, whereas if n_i were large the image would be similar to that of Figures 8 and 9. The equivalent triangular transmission for large n_i is given by the dashed line. To the right we indicate allowed transmission paths for radiation at several incident angles to illustrate the dependence of 'image' position upon incident angle. The geometry of this collimator was derived from the equations in the text.

k = grid number; $K = k_{max}$: total number of grids in collimator; d_k = diameter of wires in grid k; x_0 = linear separation between images for incident parallel radiation; x = image position relative to image position for normally incident wave; n_k = number of wires in the distance x_0; D_k = separation distance between grids 1 and k; θ = angle of incidence of impinging radiation; θ_0 = angular equivalent of image spacing x_0; θ_r = response angle: FWHM of triangular response to parallel radiation; x_r = spatial distance in image plane corresponding to θ_r; θ_{max} = limiting angle at which a source may be viewed; t = average fractional transmission of grid system; and W = width of collimator, or length of each grid.

If we first adopt values for n_1, d_1, D_2, and K, we have, for $n_1 > 2^{K-2}$ and $k > 1$:

$$\begin{aligned} x_0 &= 2d_1 n_1 \\ n_k &= n_1 - 2^{k-2} \\ d_k &= n_1 d_1/(n_1 - 2^{k-2}) \\ D_k &= 2^{k-2} D_2 (n_1 - 1)/(n_1 - 2^{k-2}). \end{aligned}$$

Note that if $n_1 \gg 2^{k-2}$ the grid separations D_k are identical to those of the multigrid collimator.

The grids must be aligned in the lateral direction so that there is one path which traverses each grid midway between two wires. The grid spacings D_k and wire densities n_k given above insure that such a path exists for all other possible angles, θ. Proper alignment is illustrated in Figure 19. From the geometry of this figure, we next obtain a relation between the angle of incidence and the image position:

$$\tan\theta = x/\{D_2(n_1 - 1)\}.$$

Note that for small angles, the quantity $D_2(n_1 - 1)$ corresponds to a focal length. Now, since the multiple image positions for a parallel beam are separated by the distance x_0, we can solve this equation for the angle that corresponds to this displacement:

$$\theta_0 \equiv \arctan\{x_0/D_2(n_1 - 1)\} = \arctan 2d_2/D_2.$$

Thus, only objects of angular size less than θ_0 will be imaged unambiguously. Finally, as mentioned above, we expect the image pattern produced by an incident plane wave to resemble that illustrated in Figure 9. The average local transmission of the collimator is a function of position and is derived from the fractional transmitting or open area in the region of concern, and, as in Figures 8 and 9, is triangular in shape. Its full width at one-half maximum and the corresponding angle are:

$$\begin{aligned} x_r &= x_0/2^{K-1} \\ \tan\theta_r &= x_0/\{2^{k-1} D_2 (n_1 - 1)\} = \tan\theta_0/2^{K-1}. \end{aligned}$$

The average transmission, t, of the collimator is $(\frac{1}{2})^K$ when n_1 is large and, for the two-dimensional collimator,

$$t = (\tfrac{1}{2})^{2K}.$$

The field of view of the instrument is limited only by its overall dimensions, that is

$$\tan\theta_{\max} = \frac{W}{D_K}.$$

In the initial choice of values for the constants, d_1, n_1, D_2, and K, one notes that (1) d_1 can be as small as is mechanically practical unless diffraction effects become a further constraint, (2) n_1 yields x_0, the separation distance between images, (3) D_2 with n_1 provides the focal length, (4) K, the total number of grids, determines, for small θ, the ratio of the FWHM response angle θ_r to the angle of image separation θ_0 and (5) a decrease in this ratio results in a decrease in the average transmission, t, of the grid system.

We assembled a two-dimensional optical model of the image forming collimator with the following parameters: $K=6$, $d_1=.07$ cm, $x_0=7$ cm, $D_2=9$ cm, and $W=10$ cm.

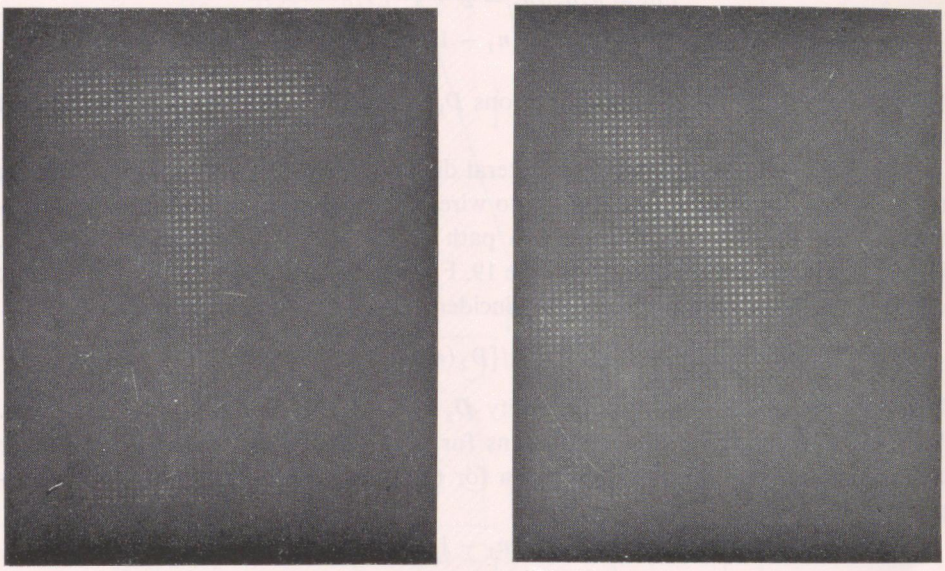

Fig. 20. Photographic images of a diffuse 'T'-shaped optical source (at a finite distance) formed by a two-dimensional image forming collimator (positive reproduction). The height of the images is about 5 cm. Dimensions of the collimator and source are given in the text.

Each grid was a glass plate with opaque lines photographically imprinted upon it. An optical object consisting of a diffuse light source in the shape of a '*T*' and of height 4 cm was placed at a distance of 9 m from the front grid of the collimator. Two of the resultant images are presented in Figure 20.

It should be noted that sources at finite distances yield image sizes and spacings which are somewhat different than those predicted herein for sources at infinity. This arises from simple geometrical considerations which take into account that each point of a close diffuse source gives rise to non-parallel rays impinging upon the collimator. However these considerations also indicate that, except for the altered sizes

and spacings of the images, the collimator as described herein properly forms images of close sources as well as of distant objects. Also, it is possible to construct an image forming collimator of grids with increasing densities of wires, that is $n, n+1, \ldots n+m$, rather than with decreasing densities as described above. If n is large, the grid spacings, focal lengths, etc., are identical for both cases. However, in the '$n+m$' case the image is inverted as in a pinhole camera whereas it is upright in the '$n-m$' case (see Figure 18). Also, the correction factors n_1-1 and n_1-2^{k-2} in the above equations become n_1+1 and n_1+2^{k-2} in the case of the '$n+m$' collimator. Our optical model was based on the '$n+m$' principle. It turned out that the collimator geometry and the source distance were such that only one of the expected multiple images occurred in the field of view (Figure 20).

Appendix: Optical Properties of Multigrid Systems

In the preceding sections, we have made reference to the optical properties of the modulation collimator in several contexts: (1) the visual observation of a diffuse light source through a collimator in order to carry out the alignment of the grids (Figure 6), (2) the photography of a diffuse light source through the collimator in order to relate the X-ray planes of maximum transmission (PMT) to the star field (Figure 13), and (3) the photography of stars through the collimator, again to relate the PMT to the celestial star field.

The optical diffraction patterns for incident diffuse white light are complex and colorful. Certain characteristics of these patterns, as viewed or photographed with focus at infinity, are:

(1) The color pattern is cyclic with an angular period equal to the angle between adjacent PMT and, furthermore, is symmetric about those PMT which are nearly normal to the grid planes. This implies that images of these patterns on black and white film will also exhibit a similar periodicity and symmetry. This result is expected from the geometrical symmetries of the collimator. However, we have also verified it experimentally (Figures 16 and 17).

(2) The pattern also exhibits symmetry about the directions midway between adjacent PMT (Figure 17). It is not readily apparent which set of symmetry angles correspond to the PMT, and calibration experiments with X-ray and optical beams must be carried out. The experiment described in Section 4 and illustrated in Figure 16 serves this purpose.

(3) The symmetries in the patterns cease to exist at angles other than those nearly normal to the grids. In the case of the 65 cm four-grid flight collimator (Figure 4) the asymmetry is less than 5% for directions 0°.5 from the normal. At 3° the asymmetry is quite severe (Figure 14). It is important not to use these asymmetric patterns to determine the location on film of a PMT at large angles unless careful X-ray-optical calibrations are carried out at these angles. The same result may be accomplished, however, by a single careful calibration in the central symmetric region coupled with direct and independent determinations of the camera's focal length and the angular

separation between adjacent PMT. This enables one to obtain the position on the film of any PMT with good accuracy.

(4) The patterns are very sensitive to the distances between grids. This is evident from a comparison of the 'short' and 'long' patterns in Figures 14 and 17 wherein the overall length of the two four-grid collimators differs by only 5%. In the case of a bigrid collimator, the pattern effectively disappears for certain separations. We have found an empirical relation for the grid spacings, D_n, which yield the most contrast in the diffraction patterns for diffuse light of wavelength λ incident upon a bigrid collimator:

$$D_n = 4nd^2/\lambda,$$

where d is the wire diameter, $2d$ is the center-to-center spacing between wires, and n an integer $\geqslant 1$ with values up to as much as 25. At these spacings the interference angle $(\lambda/2d)$ equals the modulation angles $n\theta_0 = 2nd/D$ of the collimator. High resolution systems may have values of $n > 25$ where we have not verified this expression. Good contrast can also be obtained for low resolution systems if n has certain fractional values, e.g. 0.25. In general, it is important to assemble a model of a collimator prior to its final design to insure that the optical patterns do not disappear at the proposed grid spacings.

Attempts to photograph stars through the grids also encounter diffraction effects. As illustrated in Figure 5, a 'point' source at infinity gives rise to three bright images. It turns out that these three images are those expected from the Fraunhofer diffraction of parallel, monochromatic light waves by a single grid with center-to-center wire spacing equal to twice the wire diameter. Measurements indicate that, for a four-grid collimator of length 65 cm and wire diameter 62μ, the intensity in the central maximum is about 10^{-4} that of the incident radiation, and, for wire size 125μ, about 3×10^{-3}. Clearly photography of stars through the collimators during a short rocket flight is not practical unless the density of wires and the number of grids is significantly less than in these examples.

It is not possible to write an exact analytical expression for the intensity pattern from a diffuse illumination, even for a simple bigrid collimator. This is because the second grid is at a finite distance from the first, and thus the light emitted by a single slit in the first grid does not enter the second grid as a plane wave. We have found it possible to compute the transmitted angular intensity pattern for a system of two grids using Kirchoff's formulation of the diffraction problem (BORN and WOLF, 1959). We let the first grid be illuminated by a uniform incoherent light source (e.g. Figure 6). Thus we were able to take each slit of the first grid as a light source independent in phase from the other slits of the same grid. The second grid diffracts this radiation which is then observed with a telescope focused at infinity. The resultant angular diffraction pattern was calculated for several grid separations $D = 4nd^2/\lambda$ where n is now allowed to assume non-integer values and, as before, is the multiple-slit interference angle $\lambda/2d$ in units of θ_0. The diffraction pattern depends only upon the value of n, but to fix our ideas we take $\lambda = 5900$ Å, $d = 100\mu$, and values of n which yield values of D from 7 cm to 28 cm.

The results of these calculations are presented in Figure 21. The intensity is plotted as a function of angle from 0 to $\theta_0/2$ where zero angle is a plane of maximum transmission (PMT) for X-rays. Note that for n close to an integer, the intensity contrast with angle is quite pronounced whereas at intermediate values of n the pattern increases in complexity and decreases in contrast. For increasing integer values of n,

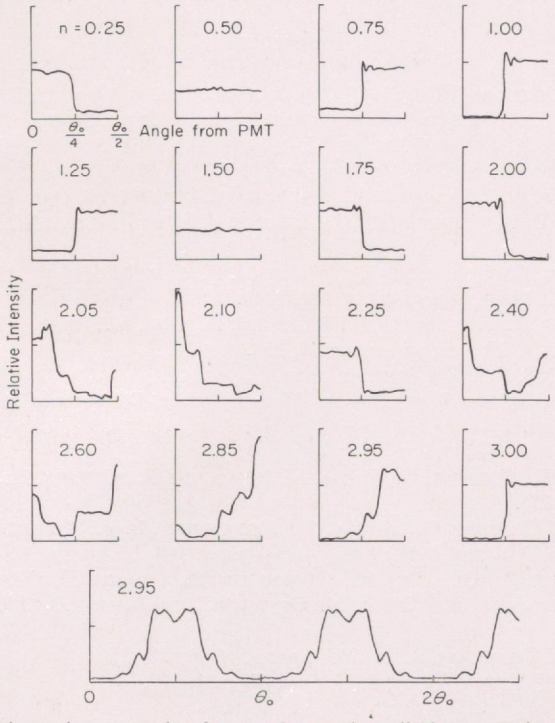

Fig. 21. Calculated intensity vs. angle of monochromatic radiation emerging from a bigrid system for various values of the parameter $n = (\lambda/2d)/(2d/D) = \lambda D/4d^2$. For wavelength $\lambda = 5900$ Å and wire diameter $d = 100\mu$, the grid spacing is $D = 6.8\,n$ cm. The radiation incident upon the various slits of the first grid is diffuse and incoherent. The emerging radiation, after diffraction by the second grid, is viewed by a telescope focused to infinity. The pattern is cyclic with a period of $\theta_0 = 2d/D$ as shown for the case $n = 2.95$. Note the pronounced variation of intensity with angle for integer values of n. The direction of the several PMT are indicated by the angles $0, \theta_0, 2\theta_0$, etc. on the abscissa.

the intense portion of the pattern alternates between 0° and $\theta_0/2$, that is, between the PMT and the anti-PMT. Finally we note that small changes in the grid spacings D lead to marked changes in the patterns.

These results reemphasize the importance of absolute X-ray-optical calibrations of a given experiment. We have not carried out the much more complex calculations for the multigrid collimator.

Acknowledgements

The authors wish to thank the entire staff of the Laboratory for Nuclear Science at Massachusetts Institute of Technology and of American Science and Engineering for

their support during this work. They are particularly grateful to Mr Edward Boughan, Mr Albert DeCaprio, Mr William Mayer, and Mr William Smith for their assistance in the development and in the understanding of the modulation collimator. Also they are indebted to Professor George Clark and Professor Bruno Rossi of M.I.T. and to Dr Giacconi of AS & E for many helpful discussions.

References

BEDO, D. E. and HINTEREGGER, H. E.: 1965, *Jap. J. Appl. Phys.* **4**, *Suppl.* I, 473.
BORN, M. and WOLF, E.: 1959, *Principles of Optics*, Pergamon Press, New York.
BOWYER, S., BYRAM, E. T., CHUBB, T. A., and FRIEDMAN, H.: 1964, *Science* **146**, 912.
GIACCONI, R. and ROSSI, B.: 1960, *J. Geophys. Res.* **65**, 773.
GIACCONI, R., HARMAN, N. F., LACEY, R.F., and SZILAGI, Z.: 1965a, *J. Opt. Soc. Am.* **55**, 345.
GIACCONI, R., REIDY, W.P., ZEHNPFENNIG, T., LINDSAY, J.C., and MUNEY, W.S.: 1965b, *Astrophys. J.* **142**, 1274.
GURSKY, H., GIACCONI, R., GORENSTEIN, P., WATERS, J. R., ODA, M., BRADT, H., GARMIRE, G., and SREEKANTAN, B. V.: 1966a, *Astrophys. J.* **144**, 1249.
GURSKY, H., GIACCONI, R., GORENSTEIN, P., WATERS, J. R., ODA, M., BRADT, H., GARMIRE, G., and SREEKANTAN, B. V.: 1966b, *Astrophys. J.* **146**, 310.
MCGRATH, J.F.Jr.: 1968, *Rev. Sci. Instr.*, in press.
MERTZ, L.: *Proceedings of the Symposium on Modern Optics*, Polytechnic Institute of Brooklyn, March 1967, in press.
ODA, M.: 1965, *Appl. Opt.* **4**, 143.
ODA, M., CLARK, G. W., GARMIRE, G., WADA, M., GIACCONI, R., GURSKY, H., and WATERS, J. R.: 1965, *Nature* **205**, 554.
ODA, M., BRADT, H., GARMIRE, G., SPADA, G., SREEKANTAN, B. V., GURSKY, H., GIACCONI, R., GORENSTEIN, P., and WATERS, J. R.: 1967, *Astrophys. J.* **148**, L5.
SANDAGE, A. R., OSMER, P., GIACCONI, R., GORENSTEIN, P., GURSKY, H., WATERS, J., BRADT, H., GARMIRE, G., SREEKANTAN, B. V., ODA, M., OSAWA, K., and JUGAKU, J.: 1966, *Astrophys. J.* **146**, 316.
SCHNOPPER, H.W. and THOMPSON, R.I.: 1968, *Space Sci. Rev.* **8**, 534.
UNDERWOOD, J. H. and MUNEY, W. S.: 1967, *Solar Phys.* **1**, 129.